In-vitro stem cell modelling demonstrates a proof-of-concept for excess functional mutant *TIMP3* as the cause of Sorsby Fundus Dystrophy

Heidi Hongisto[1,2]†, Jennifer M. Dewing[3]†, David R. G. Christensen[3], Jennifer Scott[3], Angela J. Cree[3], Janika Nättinen[4], Juha Määttä[4], Antti Jylhä[4], Ulla Aapola[4], Hannu Uusitalo[4,5], Kai Kaarniranta[1,6], J. Arjuna Ratnayaka[3], Heli Skottman[2*], Andrew J. Lotery[3*]

[1]Department of Ophthalmology, Institute of Clinical Medicine, University of Eastern Finland, Kuopio, Finland

[2]Faculty of Medicine and Health Technology, BioMediTech, Tampere University, Tampere, Finland

[3]Clinical and Experimental Sciences, Faculty of Medicine, University of Southampton, United Kingdom

[4]SILK, Department of Ophthalmology, Faculty of Medicine and Health Technology, Tampere University, Tampere, Finland

[5]Tays Eye Centre, Tampere University Hospital, Tampere, Finland

[6]Department of Ophthalmology, Kuopio University Hospital, Kuopio, Finland

[*]**Correspondence to:** AJ Lotery, Clinical & Experimental Sciences, The University of Southampton, Southampton, United Kingdom (LD74, South Lab & Path Block, Southampton General Hospital, Southampton, Hampshire, UK, SO16 6YD). E-mail: A.J.Lotery@soton.ac.uk

† Authors contributed equally

* Authors contributed equally

Running title: SFD-hiPSC-RPE demonstrate a mutant TIMP3 driven gain of function

Conflict of interest statement: No conflicts of interest were declared.

Word count: 3969

Abstract

Sorsby Fundus Dystrophy (SFD) is a rare autosomal dominant disease of the macula that leads to bilateral loss of central vision and is caused by mutations in the *TIMP3* gene. However, the mechanisms by which *TIMP3* mutations cause SFD are poorly understood. Here, we generated human induced pluripotent stem cell-derived retinal pigmented epithelial (hiPSC-RPE) cells from three SFD patients carrying *TIMP3 p.(Ser204Cys)* and three non-affected controls to study disease related structural and functional differences in the RPE. SFD-hiPSC-RPE exhibited characteristic RPE structure and physiology but showed significantly reduced transepithelial electrical resistance associated with enriched expression of cytoskeletal remodelling proteins. SFD-hiPSC-RPE exhibited basolateral accumulation of TIMP3 monomers, despite no change in *TIMP3* gene expression. TIMP3 dimers were observed in both SFD and control hiPSC-RPE, suggesting mutant TIMP3 dimerization does not drive SFD pathology. Furthermore, mutant TIMP3 retained matrix metalloproteinase activity. Proteomic profiling showed increased expression of extracellular matrix proteins, endothelial cell interactions and angiogenesis-related pathways in SFD-hiPSC-RPE. By contrast, there were no changes in VEGF secretion. However, SFD-iPSC-RPE secreted higher levels of monocyte chemoattractant protein 1, platelet-derived growth factor, and angiogenin. Our findings provide a proof-of-concept that SFD patient-derived hiPSC-RPE mimic mature RPE cells and support the hypothesis that excess accumulation of mutant TIMP3, rather than an absence or deficiency of functional TIMP3, drives ECM and angiogenesis related changes in SFD.

Keywords: Sorsby fundus dystrophy, human induced pluripotent stem cell, retinal pigment epithelial cell, retinal degeneration, metalloproteinase inhibitor 3

Introduction

Sorsby fundus dystrophy (SFD) is a rare, autosomal dominant macular dystrophy caused by mutations in the gene *TIMP3* (metalloproteinase inhibitor 3) and is estimated to affect 1 in 220,000 people [1]. Without genetic testing, SFD patients are often misdiagnosed with either idiopathic choroidal neovascularization or wet age-related macular degeneration (AMD) due to their shared clinical features. However, onset of the disease occurs earlier in SFD patients, usually between the 4th and 6th decade of life [1,2]. Rare variants of *TIMP3* have been identified in genome wide association studies (GWAS) of AMD [3]. However, the causative relationship between *TIMP3* variants and AMD risk alleles remains ambiguous. SFD patients experience bilateral loss of central vision due to atrophy of the retinal pigmented epithelium (RPE) or choroidal neovascularisation (CNV), leading to irreversible photoreceptor loss. Initially, patients show lipid-enriched, drusen-like deposits between the basement membrane of the RPE and the inner-collagenous layer of Bruch's membrane (BrM) [4]. The RPE and the underlying BrM are the epicentre of SFD development. Together they form the outer blood-retina barrier (BRB) which selectively regulates the transport of nutrients and waste between the retina and the choriocapillaris. A markedly thickened BrM is a key feature observed in SFD patients and is believed to impair diffusion across the BRB and contribute to the accumulation of RPE metabolic waste products and the subsequent formation of sub-RPE deposits [5,6]. Current treatments for SFD patients focus on managing CNV through regular intravitreal vascular endothelial growth factor (VEGF) inhibitor injections to limit choroidal pathology [7].

The family of TIMP proteins are expressed ubiquitously within the body and play a myriad of biological roles through their ability to reversibly inhibit MMPs (matrix metalloproteinases), ADAMs (a disintegrin and metalloproteinase) and ADAMTS (a

disintegrin and metalloproteinase with thrombospondin motifs) [8,9]. *TIMP3* encodes a 24 kDa glycoprotein consisting of two domains: the N-terminal domain is involved in MMP inhibition (and at high levels can induce apoptosis in RPE), whereas the C-terminal domain binds directly to VEGFR2 (KDR), inhibiting VEGF binding and downstream PI3K/Akt and Ras/Raf/ERK signalling in choroidal endothelial cells [1]. Of the four members of the TIMP family, TIMP3 possesses the broadest range of activity, including the ability to inhibit all MMPs and several of the ADAM and ADAMTS family [8]. To date, 18 SFD-causing *TIMP3* mutations have been identified, with the majority occurring at the C-terminus of the protein and resulting in the gain or loss of a cysteine residue. The current hypothesis proposes this odd number of cysteines enables formation of intermolecular disulphide bridges between mutated TIMP3 proteins, resulting in dimers or multimers that are more resistant to turnover/clearance from the ECM, and thus contributes to thickening of BrM [1].

Whilst several studies have shown that mutant TIMP3 retains its MMP inhibitory function, others have reported a loss-of-function phenotype. Thus, it remains unclear how mutations in *TIMP3* affect the resulting protein's ability to regulate ECM assembly/disassembly (reviewed in [1,2]). Several studies were also unable to confirm dimerization of mutant TIMP3 [10,11]. These inconsistencies are likely due to differences in the *TIMP3* mutation of interest and the cell types used to study them. Of note, not all known SFD *TIMP3* mutations result in a loss or gain of a cysteine, with some mutations generating novel lysine or arginine residues or indeed a premature stop codon. This suggests that alternative structural changes to the TIMP3 protein may underlie disease phenotypes in these patients [1]. Despite being a monogenetic disorder, there is considerable heterogeneity between SFD patients depending on the TIMP3 mutation, and indeed even within families with the same mutation [1,2]. Mouse

models of SFD have been unable to successfully recapitulate the phenotypic severity observed in SFD patients. Knock-in mice (*Timp3*$^{+/S156C}$, *Timp3*$^{S156C/S156C}$) have been shown to exhibit abnormalities of BrM and the basal microvilli at 8 months of age, compared to 30 months in wild-type littermates; however, electrophysiology demonstrates normal retinal function [12].

The shortcomings of current *in vitro* and animal models necessitate the development of new approaches to elucidate underlying disease mechanisms. Human induced pluripotent stem cells (hiPSCs) enable relevant, patient-specific disease modelling and have provided novel insights into drusen biogenesis in rare retinal dystrophies [13]. In view of the aforementioned limitations, we established hiPSC-RPE cell lines from three TIMP3 p.(Ser204Cys) SFD patients and healthy controls to determine how this mutation alters the structure and function of RPE cells.

Materials and methods

Detailed methodology is provided in Supplementary materials and methods.

Ethics

The University of Southampton has ethical approval for SFD hiPSC generation (UK REC reference: 14/LO/1330, 23.06.2014). Participation was voluntary, and patients gave written informed consent. Tampere University has an appropriate licence of The Board for Gene Technology, Finland (022/M/2016, 20.06.2016) and ethical approval of the Ethical Committee of Pirkanmaa Hospital District to derive (R08070, 11.10.2016; R12123, 3.10.2017) and conduct studies with hiPSC lines (R14023, 13.12.2016). The Declarations of Helsinki were adhered to.

Patients

After ethical approval and informed consent, skin biopsies were obtained from three SFD patients from Southampton General Hospital, UK:
TIMP3 c.610A>T; p.(Ser204Cys), confirmed by genotyping. Two of the three SFD patients were sisters. Skin biopsies were also taken from the unaffected mother of the sisters, who served as a control. In addition, two control hiPSC lines from unaffected individuals were kindly provided by Professor Aalto-Setälä, Tampere University, Finland. All patient information was pseudonymised for analysis.

Human iPSC-RPE

Fibroblasts isolated from patient skin biopsies were reprogrammed into human iPSCs using CytoTune-iPS Sendai Reprogramming kit (Thermo Fisher Scientific, Waltham, MA, USA) according to the manufacturer's instructions. Two clones per patient and one

clone per control were further cultured and characterized (Table 1), as described in detail in the Supplementary materials and methods. RPE differentiation was performed using spontaneous differentiation, followed by RPE selection, sequential passaging for purification and expansion, cryopreservation, and final maturation on permeable cell culture inserts (Cat. MCRP24H48, Merck Millipore, Darmstad, Germany) or in 24-well plates (Corning® CellBIND®, Merck Millipore) at passage 4 (P4). Human iPSC-RPE clones (n=3 control, and n=5 SFD) were characterized for expression of cell-specific markers, transepithelial electrical resistance (TEER), polarized secretion of pigment epithelium-derived factor (PEDF) and phagocytic capacity.

Transmission electron microscopy

For transmission electron microscopy (TEM) analysis, hiPSC-RPE (n=3 control, n=3 SFD) were cultured on inserts for 71–81 days. Details of sample preparation have been described previously [14].

RT-qPCR

Relative *TIMP3* gene expression between control (n=3) and SFD-hiPSC-RPE (n=5 SFD, day 73) was analysed using RT-qPCR using TaqMan Gene Expression Assay HS00165949_m1 (Applied Biosystems, Thermo Fisher Scientific).

Western blotting

Western blotting (WB) was used to investigate the expression of TIMP3 (1:750, ab39184 and ab58804 both from Abcam, Cambridge, UK), Apolipoprotein E (1:1000, ab947, Millipore), Fibulin (1:400, sc-33722, Santa Cruz Biotechnology, Dallas, Texas, USA), and β-Actin (1:1000, sc-47778, Santa Cruz Biotechnology) in hiPSC-RPE (n=3 control, n=5 SFD, 70–76 days) under reducing conditions.

Enzyme-Linked Immunosorbent Assay (ELISA)

Secretion of PEDF (DY1177-05, R&D Systems, Minneapolis, Canada), TIMP3 (ab119608, Abcam), and VEGF (DVE00, R&D Systems) by hiPSC-RPE (n=3 control, n=5 SFD) was quantified using enzyme-linked immunosorbent assays (ELISA).

Collagenase assay

MMP-inhibitory activity of conditioned medium (CM) of hiPSC-RPE (n=3 control, n=5 SFD) was examined in triplicate using a collagenase activity assay (EnzChek gelatinase/collagenase kit; Thermo Fisher Scientific).

Sequential window acquisition of all theoretical mass spectra (SWATH-MS) proteomics

For mass spectrometry proteomics, the hiPSC-RPE were cultured for 70 days on 24-well plates (n=3 control, n=5 SFD and 3–7 replicates/cell line). The cells were initially pelleted and frozen at –80 °C. For MS analysis cell pellets were lysed and total protein concentration of each sample was measured, after which proteins were reduced, alkylated and digested with trypsin as described previously [15,16]. Analysis of the samples was performed using an Eksigent 425 NanoLC coupled with high speed TripleTOF 5600+ mass spectrometer (Ab Sciex, Concord, Canada) using SWATH acquisition as described previously [15,16].

Human angiogenesis array

Secretion of angiogenesis-related proteins was analysed in pooled basal culture medium from hiPSC-RPE cells cultured on inserts (n=3 control, n=5 SFD, 2 inserts

each) using the Proteome Profiler Human Angiogenesis Array Kit (ARY007, R&D Systems).

Results

Sorsby Fundus Dystrophy patient-derived hiPSC lines

Human iPSC lines were generated from three female individuals diagnosed with SFD and carrying *TIMP3* mutation producing p.(Ser204Cys) (previous nomenclature p.(Ser181Cys)) (Table 1). Two of the patients were siblings, the other was unrelated. The mother of the two sisters, who is unaffected with no history of macular degeneration, served as a healthy control, in addition to two healthy, unrelated, age-matched females. Despite anti-VEGF treatment over a 11-year period, SFD pathology progressed, with the development of macular scarring due to ongoing CNV (Figure 1). Two hiPSC clones from each patient were cultured and extensively characterized (Table 1). The removal of the introduced viral vectors and the presence of the disease-causing *TIMP3* missense mutation was confirmed in the hiPSCs. These cells exhibited pluripotency and normal diploid karyotype (46, XY), except for two of the SFD clones (RD01A and RD03B) that showed balanced translocations (supplementary material, Figures S1–S5), which had no effect on hiPSC phenotype.

SFD-hiPSC-RPE had normal RPE properties and functionality but showed a compromised barrier after 10 weeks in culture

The hiPSC cells were differentiated into RPE. The protocol and timeline for differentiation is shown in Figure 2A. The cell lines revealed clear clone-specific differences in differentiation capacity, with RD04B failing to produce sufficient pigmented RPE (in five separate differentiation experiments) to warrant further selection and expansion. All other clones produced functional, polarized RPE monolayers on porous inserts (Figure 2). We used a 10-week long-term culture to age the cells and allow phenotypic changes to manifest. Significantly lower ($p=0.0095$, Mann–Whitney test) average TEER was recorded for SFD-hiPSC-RPE compared to

controls (Figure 2C), although clone-specific differences in mean TEER were seen. All cell lines showed intact junctional localization of zonula occludens 1 (ZO1) (Figure 2D) and a normal RPE protein marker profile (supplementary material, Figure S6). All hiPSC-RPE lines demonstrated the capacity to phagocytose photoreceptor outer segments (POS) (Figure 2E), with no difference in the number of attached (total, p=0.7, Mann–Whitney test) or internalised (p=1.0) POS between control and SFD-hiPSC-RPE (Figure 2F). PEDF was secreted in a polarized manner with >4-fold higher secretion to the apical insert compartment compared with the basolateral chamber for both control and SFD-hiPSC-RPE (Figure 2G). The hiPSC-RPE bearing karyotypic translocations (RD01A and RD03B) showed comparable RPE properties to karyotypically normal SFD-hiPSC-RPE cell lines (Figure 2C,G, and supplementary material, Figure 7) and were therefore included in the subsequent analyses.

SFD-hiPSC-RPE show similar fine structure to controls

The ultrastructure of hiPSC-RPE monolayers cultured on permeable inserts for 70 days was analysed by TEM. Cells were found to be polarized in a typical apical-basal axis and showed characteristic RPE structures including apical microvilli, melanosomes, basal nuclei and basolateral infolds, as well as sub-RPE deposits (Figure 3A). No difference in cell height (p=0.7477, unpaired, two-tailed *t*-test) (Figure 3A,B), average length of apical microvilli (p=0.9) (Figure 3A,C), or average basal lamina thickness (p=0.6387) (Figure 3D,E) were found between SFD and control-hiPSC-RPE. Sub-RPE deposits with a distinct striated pattern were identified as fibrous long-spacing (FLS) collagen and were observed between RPE and the underlying insert surface in all samples (Figure 3F, arrows). No difference in the number of FLS collagen deposits per cell was observed between SFD and control hiPSC-RPE (p=0.8389) (Figure 3G). The

number of melanosomes per cell (open arrow) was also similar between SFD and control hiPSC-RPE (Figure 3H,I) (p=0.6065).

SFD-hiPSC-RPE retained the capacity to inhibit MMPs but showed basolateral accumulation of TIMP3

Expression, secretion, accumulation, and functionality of TIMP3 was investigated in hiPSC-RPE lines cultured for 70–84 days on 24-well plates. RT-qPCR analysis showed no difference (p= 0.2500, Mann–Whitney test) in *TIMP3* transcript levels in SFD-hiPSC-RPE compared to controls (Figure 4A). However, WB under reducing conditions showed significantly higher expression levels (8.6-fold difference, p=0.0357) of monomeric TIMP3 in SFD-hiPSC-RPE (21 kDa expected band size for ab39184) (Figure 4B). A larger sized band which was interpreted as 27 kDa glycosylated form, and another 48 kDa band, which was interpreted as a TIMP3 dimer, were found in all cell lines. We observed a similar pattern of significantly increased monomeric TIMP3 expression in SFD-hiPSC-RPE using an alternative TIMP3 antibody (Abcam ab58804) (supplementary material, Figure 8B,C). SFD-hiPSC-RPE showed slightly more TIMP3 glycosylation and dimerization in some of the blots, but the changes were not consistent in all replicate immunoblots (Figure 4B, supplementary material, Figure 8A–C). To investigate differences in the secretion of TIMP3, an ELISA assay was carried out, which showed SFD-hiPSC-RPE lines secreted significantly less TIMP3 compared to controls (p=0.0357) (Figure 4C). An ELISA was also performed on apical and basal conditioned medium (CM) collected from cells cultured on permeable culture inserts. TIMP3 was secreted predominantly via the basolateral surface in both control and SFD-hiPSC-RPE. However, basal secretion was significantly greater compared to apical secretion in SFD-hiPSC-RPE, but not in controls (p=0.0357) (supplementary material, Figure 8D).

The MMP-inhibitory activity of TIMP3 was compared between SFD-hiPSC-RPE and controls. CM was collected from cells cultured in 24-well plates and analysed using an EnzChek collagenase assay. The assay uses quenched, fluorescein-labelled gelatin that is digested by collagenase from *Clostridium histolyticum* leading to increased fluorescence proportional to proteolytic activity. Collagenase activity was moderately inhibited by the CM (containing 50 pg total TIMP3) from both SFD-hiPSC-RPE and control-hiPSC-RPE up to 3 h. However, a significant reduction in collagenase activity was seen in CM from SFD-hiPSC-RPE compared to controls by 20 ($p=0.0357$) and 26 h ($p=0.0357$), respectively (Figure 4D, supplementary material, Figure S9).

Extracellular matrix, cytoskeleton, angiogenesis, and endothelial cell-related pathways and proteins were differentially regulated between control- and SFD-hiPSC-RPE

A quantitative whole cell proteomic profiling of the hiPSC-RPE was conducted to compare the changes in cellular proteome caused by mutant TIMP3. Out of 2585 candidate proteins, 1638 were included in the analyses after coefficient of variation (CV) filtering, removing proteins with mean CV>30%. Out of the 1638 candidates, 89 proteins were differentially regulated according to fold-change (≥1.5-fold up- or down-regulated) in the SFD-hiPSC-RPE compared to controls (supplementary material, Table S1, Figure S10A). Interestingly, ECM and ECM-remodelling proteins were upregulated, including collagen α1 chains (COL1A1, COL12A1, COL18A1, COL14A1), nidogen 2 (NID2), laminin subunit gamma 1 (LAMC1), and peroxidasin (PXDN). Functional analysis based on the DAVID bioinformatics tool, connected the differentially regulated proteins to ECM, cytoskeleton, cell adhesion, and cell junctions (supplementary material, Figure S10B). A known TIMP3 binding partner EGF-

containing fibulin-like extracellular matrix protein 1 (EFEMP1, also known as fibulin 3), and a known drusen constituent apolipoprotein E (APOE), were shown to be upregulated and were verified by WB (supplementary material, Figure S10 C–H). TIMP3 (initially filtered out due to variation) was upregulated 1.7-fold in SFD-hiPSC-RPE (supplementary material, Figure S11). Next, a statistical analysis using a two-level nested ANOVA model was performed to compare differences in protein expression between SFD and control-hiPSC-RPE. The model provided a coefficient equivalent to fold-change for each comparison and revealed that 156 proteins were differentially regulated ($p<0.05$) in SFD-hiPSC-RPE compared to controls (supplementary material, Table S2). These results were used to perform Ingenuity Pathway Analysis which revealed upregulation of pathways associated with endothelial cell functions and interactions, as well as upregulation of cytoskeleton remodelling in the SFD-hiPSC-RPE (Figure 5A, supplementary material, Table S3). Upstream regulators for these pathways such as transforming growth factor beta 1 (TGFβ1), tumour necrosis factor (TNF), and peroxisome proliferator-activated receptor gamma (PPARG) were also identified (Figure 5B, and supplementary material, Table S4). As differential regulation of angiogenesis was revealed, secretion of angiogenesis related proteins from the basal media were studied in more detail. VEGF was secreted at similar levels by both control and SFD-hiPSC-RPE ($p=0.5714$, Mann–Whitney test) (Figure 6A). Further, secretion of 55 angiogenesis-related proteins was studied using a membrane-based antibody array. The same 15 proteins were secreted at detectable levels by both SFD and control-hiPSC-RPE (Figure 6B). Relative quantitation of spot intensities showed SFD-hiPSC-RPE to secrete more monocyte chemoattractant protein 1 (MCP-1/CCL2, 3.1-fold intensity), one of the key chemokines that regulate migration and infiltration of monocytes/macrophages, higher levels of platelet-derived growth factor (PDGF-AA, 1.5-fold intensity), as well as slightly more angiogenin (1.3-fold intensity) (Figure 6C).

Discussion

Many aspects of SFD pathophysiology remain poorly understood. Inconsistent results from previous studies have failed to resolve whether mutant TIMP3 dimerizes, retains its MMP inhibitory function and VEGFR2 binding capacity, or induces other yet unknown pathological changes [1,2]. In this study, we generated SFD patient-derived hiPSC-RPE carrying *TIMP3* mutation causing p.(Ser204Cys) to study the underlying biology of the RPE. Long-term culture for 70 d were used to age the RPE, which exhibited polarized monolayers with a characteristic RPE-specific phenotype. Although the clone-specific variations in TEER warrant some caution, the average TEER values in SFD-hiPSC-RPE lines were significantly lower compared to controls. The cell line and clone-specific differences likely represent typical inherent variability between hiPSC lines and clones, similar to those reported in other studies using iPSCs [17] but might also reflect the heterogeneity observed in SFD patients [1]. The proteomic analysis indicated enriched cytoskeletal remodelling, adhesion, and junctional proteins in SFD-hiPSC-RPE, which could explain the lowered TEER of the RPE monolayer. Cytoskeletal remodelling is critical in regulating cellular junctional integrity [18], and alterations to the actin cytoskeleton and microtubules have been shown to have a major impact on RPE and retinal homeostasis in AMD [19]. Although the hiPSC-RPE showed normal architecture with regular polygonal geometry, cell size and shape, and expression of tight junction protein ZO1, it is plausible that TIMP3 dysregulation leads to cytoskeletal reorganization. This could further induce pathological responses in the RPE cells, which warrants further investigation.

At ultrastructural level, sub-RPE deposits were identified in the form of FLS collagen, a polymorphous form of collagen defined by banding pattern periodicity greater than approximately 67 nm [20]. FLS collagen deposits have been observed under the RPE in human post-mortem eyes, suggesting they occur naturally [21]. In a previous study

by Galloway *et al* (2017), hiPSC-RPE were used to study drusen biogenesis in three retinal dystrophies, namely Malattia Leventinese (ML), autosomal dominant radial drusen (ADRD), and SFD [13]. TEM imaging revealed an increased number of basal deposits under SFD-hiPSC-RPE from two patients after 90 d of ageing *in vitro* [13]. Contrary to these findings, our study found no significant changes to the number of deposits nor thickness of the basal lamina in SFD-hiPSC-RPE (n=3). It is possible, that the highly permeable cell culture inserts of 1 µm pore size used, or differing culture conditions negatively influenced ECM thickening and accumulations in our study. Consistent with previous reports, *TIMP3* mRNA expression levels were similar between SFD and control-hiPSC-RPE, suggesting that the mutation causing p.(Ser204Cys) does not affect transcription of the *TIMP3* gene [22,23]. WB analysis confirmed significantly greater quantities of TIMP3 monomer in SFD-hiPSC-RPE lysates compared to controls; however, this did not equate to greater TIMP3 secretion. In fact, secretion of TIMP3 protein was diminished in SFD-hiPSC-RPE, suggesting the protein is retained within RPE cells or the underlying ECM. The presence of TIMP3 dimers has been shown in transfected fibroblast cell lines [24,25] and SFD patient-derived fibroblasts [23] carrying the p.(*Ser204Cys)TIMP3* mutation. However, we observed TIMP3 dimers from both SFD and control hiPSC-RPE lysates, indicating that dimerization is not unique to mutant TIMP3. The WBs also indicated a moderate increase in the abundance of the 27 kDa glycosylated form, although the results were not clear for all WBs due to the glycosylated form being less abundant than the TIMP3 monomer. Differences in TIMP3 glycosylation states for specific SFD mutants p.(Ser179Cys and Ser38Cys) have been reported [10,26]. It has been suggested that the aberrant disulphide bonding of the mutated TIMP3 could alter its binding affinity for C-terminal binding partners such as pro-MMPs, which in turn could influence glycosylation of the TIMP3 protein [10].

Results from the enzyme assay confirmed that mutant TIMP3 retains its MMP inhibiting capacity, demonstrated by a reduction in collagenase activity on a gelatin substrate in the presence of CM from SFD-hiPSC-RPE. Of note, from 20 h onwards, collagenase activity in the presence of SFD CM was significantly lower compared to controls, suggesting mutant TIMP3 exhibits greater MMP inhibition compared to its WT counterpart. MMP-2 and MMP-9 are key MMPs implicated in BrM dysregulation [27-29]. If mutant TIMP3 retains its ability to inhibit MMPs, or even exhibits increased inhibition as our data suggests, the retention of active, mutant TIMP3 in RPE and BrM may enable continuous MMP inhibition and subsequent increase in ECM synthesis (reduced ECM turnover). This theory is consistent with BrM thickening as a key hallmark of SFD pathology [30].

Proteomic profiling indicated enriched expression of many ECM proteins in SFD-hiPSC-RPE, consistent with increased adhesiveness of the mutant TIMP3 to the ECM [25]. One such protein was EFEMP1 (Fibulin 3), a known TIMP3 binding partner. Mutations in *EFEMP1* lead to the rare macular autosomal dominant disease ML, which shares striking similarities with SFD and AMD [31]. EFEMP1 is an extracellular glycoprotein expressed in the basement membranes of epithelial and endothelial cells, including the BrM. EFEMP1 stimulates the expression of TIMP3 but inhibits expression of MMP-2 and MMP-9 [32]. Mutated EFEMP1 has been shown to misfold and accumulate within RPE cells and contribute to drusen formation in ML [33-35]. EFEMP1 also has a role in regulating angiogenesis [36]. Our results suggest possible accumulation of TIMP3–EFEMP1 complexes [37] which could further promote inhibition of MMPs and contribute to the build-up of toxic deposits, augment angiogenesis, and cause chronic activation of the alternative complement pathway [38,39]. This theory is supported by the data from our IPA data that identified endothelial cell migration and angiogenesis as key pathways associated with the 156 significantly differentially-

expressed proteins observed in SFD hiPSC-RPE, relative to controls. TGFβ, TNF and PPARG are upstream regulators that were identified by IPA. TGFβ and TNF are known positive regulators of many cellular processes including angiogenesis, whilst the negative regulator PPARG is a nuclear receptor transcription factor that plays an important role in the control of ocular pathophysiological processes such as anti-angiogenesis, inflammation, and oxidative stress response [40].

Moreover, SFD-hiPSC-RPE secreted increased levels of monocyte chemoattractant protein 1 (MCP1/CCL2), platelet-derived growth factor (PDGF-AA) and angiogenin. MCP1/CCL2 is linked to both inflammation and angiogenesis and is released from Müller glia and the RPE under stress conditions to attract microglia/macrophages expressing chemokine receptor 2 (CCR2) to sites of retinal damage [41]. MCP1/CCL2 polymorphisms have been linked to AMD [42,43]. Furthermore, MCP1/CCL2 has been shown to attract microglia to amyloid-β plaques in the brain and mediate their clearance in Alzheimer's disease [44]. Thus, MCP1/CCL2 may also play an important role in clearance of sub-RPE deposits, inflammation, and angiogenesis in SFD.

The C-terminal domain of TIMP3 directly binds to VEGFR2, inhibiting the binding of VEGF and the downstream signalling that regulates choroidal angiogenesis [45,46]. Our results revealed no difference in the basal secretion of VEGF by SFD-hiPSC-RPE compared to controls, suggesting that SFD-RPE continue to secrete VEGF to the underlying choroid normally. However, it is possible that accumulation of mutant TIMP3 protein within/under RPE may restrict the amount of bioavailable TIMP3 reaching the choroid, enabling VEGF-mediated proliferation and migration of endothelial cells to continue unchecked. It remains unclear whether mutant TIMP3 may be less effective at inhibiting VEGF binding to VEGFR2, favouring angiogenesis; however, the available data in this area remains contradictory [26,47,48]. Differentiation of endothelial cells from SFD-hiPSCs, and their co-culture with SFD-hiPSC-RPE could be used to

generate a patient-specific *in vitro* 3D model that mimics the RPE-choroidal interface, providing new insights into SFD pathobiology [49,50]. Furthermore, extrapolation of these findings to an hiPSC-RPE model of AMD, or with gene corrected isogenic control lines pose interesting future research directions.

Here, we have generated SFD patient-derived hiPSC-RPE carrying the *TIMP3 p.(Ser204Cys)* mutation and through extensive characterisation have confirmed they are consistent with mature RPE cells. The findings from this study offer novel insights into the molecular mechanisms underpinning SFD and suggest that accumulation and retention of functional mutant TIMP3 protein within the BrM may promote ECM thickening and choroidal angiogenesis, which drives SFD pathophysiology.

Acknowledgements

We thank Professor Katriina Aalto-Setälä (Tampere University) for providing the control hiPSC lines UTA.04311.WTs and 10211.EURCCs. We also thank laboratory technicians Outi Melin, Hanna Pekkanen, Outi Heikkilä, Emma Vikstedt, and Saara Lähdekorpi at Tampere University for excellent assistance with cell culture and analyses. We thank Dr Helen Lotery for advising on skin biopsy technique and Dr Rebecca Kaye for performing skin biopsies and some preliminary culturing of cells in Southampton. The authors acknowledge the Biocenter Finland (BF) and Tampere Imaging Facility (TIF), Tampere University, Finland, as well as the Biomedical Imaging Unit (BIU), University of Southampton, UK for their services. The study was funded by Academy of Finland (315085), Finnish Cultural Foundation, Mary and Georg C. Ehrnrooth's Foundation, Sokeain Ystävätry, Retina UK (GR590), The Alzheimer's Research UK South Coast Network and The Gift of Sight Appeal.

Author contributions statement

HH was mainly responsible for the cell culture, designing and performing the experiments, analysing, and interpreting data, and writing the manuscript. JMD made a major contribution in performing experiments, analysing and interpreting data, and writing the manuscript. DRGC participated in cell culture and optimized methods. JS contributed to cell culture and DNA extraction of hiPSC-RPE cell lines. AJC contributed to project design and management**.** JN conducted the bioinformatics for the proteomics and generated related images. JM, AJ, UA, and HU carried out the proteomics analyses and helped in data analyses. KK participated in study design and funding, JAR participated in study design, and data interpretation. HS and AJ contributed to study design, data interpretation, and provided financial and administrative support. AL

organised collection of donor patient samples. All authors were involved in writing the manuscript and had final approval of the submitted and published versions.

SUPPLEMENTARY MATERIAL ONLINE

Supplementary materials and methods

Figure S1. SFD-hiPSC characteristics

Figure S2. Characterization of the SFD-hiPSC clones RD01A and RD01C

Figure S3. Characterization of the SFD-hiPSC clones RD03A and RD03B

Figure S4. Characterization of the SFD-hiPSC clone RD04B and control-hiPSC clone RD08A (Control 1)

Figure S5. Characterization of the Control-hiPSC lines UTA.04311.WTs (Control 2) and 10211.EURCCs (Control 3)

Figure S6. RPE characteristics

Figure S7. The hiPSC-RPE bearing karyotypic translocations (RD01A and RD03B) showed similar RPE properties as the other SFD-hiPSC-RPE lines

Figure S8. TIMP3 expression and secretion

Figure S9. EnzCheck collagenase assay results shown for each cell line individually

Figure S10. Proteomic profiling of SFD-hiPSC-RPE comparing to control-hiPSC-RPE

Figure S11. TIMP3 was initially filtered out of the analysed data during stringent CV filtering

Table S1. Differentially expressed proteins according to fold change in SFD-hiPSC-RPE/Control-hiPSC-RPE

Table S2. Differentially expressed proteins according to statistical significance (LMER linear mixed effects model) in SFD-hiPSC-RPE/Control-hiPSC-RPE

Table S3. IPA pathway analysis for diseases and biological functions for the significant proteins with p-value <0.05

Table S4. Upstream regulators of the disease associated pathways

References

1. Christensen DRG, Brown FE, Cree AJ*, et al.* Sorsby fundus dystrophy - A review of pathology and disease mechanisms. *Exp Eye Res* 2017;**165:**35-46.

2. Anand-Apte B, Chao JR, Singh R*, et al.* Sorsby fundus dystrophy: Insights from the past and looking to the future. *J Neurosci Res* 2019;**97:**88-97.

3. Fritsche LG, Igl W, Bailey JNC*, et al.* A large genome-wide association study of age-related macular degeneration highlights contributions of rare and common variants. *Nat Genet* 2016;**48:**134-143.

4. Gliem M, Müller PL, Mangold E*, et al.* Reticular Pseudodrusen in Sorsby Fundus Dystrophy. *Ophthalmology* 2015;**122:**1555-1562.

5. Hussain AA, Starita C, Hodgetts A*, et al.* Macromolecular diffusion characteristics of ageing human Bruch's membrane: implications for age-related macular degeneration (AMD). *Exp Eye Res* 2010;**90:**703-710.

6. Curcio CA, Johnson M. Structure, Function, and Pathology of Bruch's Membrane. In *Retina* (5th edn). Elsevier Inc, 2012; 465-481.

7. Gemenetzi MK, Luff AJ, Lotery AJ. Successful treatment of choroidal neovascularization secondary to sorsby fundus dystrophy with intravitreal bevacizumab. *Retin Cases Brief Rep* 2011;**5:**132-135.

8. Brew K, Nagase H. The tissue inhibitors of metalloproteinases (TIMPs): an ancient family with structural and functional diversity. *Biochim Biophys Acta* 2010;**1803:**55-71.

9. Dewing JM, Carare RO, Lotery AJ*, et al.* The Diverse Roles of TIMP-3: Insights into Degenerative Diseases of the Senescent Retina and Brain. *Cells* 2019;**9:**10.3390/cells9010039.

10. Naessens S, De Zaeytijd J, Syx D*, et al.* The N-terminal p.(Ser38Cys) TIMP3 mutation underlying Sorsby fundus dystrophy is a founder mutation disrupting an intramolecular disulfide bond. *Hum Mutat* 2019;**40:**539-551.

11. Qi JH, Ebrahem Q, Yeow K*, et al.* Expression of Sorsby's fundus dystrophy mutations in human retinal pigment epithelial cells reduces matrix metalloproteinase inhibition and may promote angiogenesis. *J Biol Chem* 2002;**277:**13394-13400.

12. Weber BHF, Lin B, White K*, et al.* A mouse model for Sorsby fundus dystrophy. *Invest Ophthalmol Vis Sci* 2002;**43:**2732-2740.

13. Galloway CA, Dalvi S, Hung SSC*, et al.* Drusen in patient-derived hiPSC-RPE models of macular dystrophies. *Proc Natl Acad Sci U S A* 2017;**114:**E8214-E8223.

14. Sorkio A, Hongisto H, Kaarniranta K*, et al.* Structure and barrier properties of human embryonic stem cell-derived retinal pigment epithelial cells are affected by extracellular matrix protein coating. *Tissue Eng Part A* 2014;**20:**622-634.

15. Vähätupa M, Nättinen J, Jylhä A*, et al.* SWATH-MS Proteomic Analysis of Oxygen-Induced Retinopathy Reveals Novel Potential Therapeutic Targets. *Invest Ophthalmol Vis Sci* 2018;**59:**3294-3306.

16. Nättinen J, Jylhä A, Aapola U*, et al.* Topical fluorometholone treatment and desiccating stress change inflammatory protein expression in tears. *Ocul Surf* 2018;**16:**84-92.

17. Ortmann D, Vallier L. Variability of human pluripotent stem cell lines. *Curr Opin Genet Dev* 2017;**46:**179-185.

18. Ivanov AI, Parkos CA, Nusrat A. Cytoskeletal regulation of epithelial barrier function during inflammation. *Am J Pathol* 2010;**177:**512-524.

19. Tarau I, Berlin A, Curcio CA*, et al.* The Cytoskeleton of the Retinal Pigment Epithelium: from Normal Aging to Age-Related Macular Degeneration. *Int J Mol Sci* 2019;**20:**.

20. Paige MF, Rainey JK, Goh MC. Fibrous long spacing collagen ultrastructure elucidated by atomic force microscopy. *Biophys J* 1998;**74:**3211-3216.

21. Curcio CA, Millican CL. Basal linear deposit and large drusen are specific for early age-related maculopathy. *Arch Ophthalmol* 1999;**117:**329-339.

22. Chong NHV, Kvanta A, Seregard S*, et al.* TIMP-3 mRNA is not overexpressed in Sorsby fundus dystrophy. *Am J Ophthalmol* 2003;**136:**954-955.

23. Arris CE, Bevitt DJ, Mohamed J*, et al.* Expression of mutant and wild-type TIMP3 in primary gingival fibroblasts from Sorsby's fundus dystrophy patients. *Biochim Biophys Acta* 2003;**1638:**20-28.

24. Langton KP, Barker MD, McKie N. Localization of the functional domains of human tissue inhibitor of metalloproteinases-3 and the effects of a Sorsby's fundus dystrophy mutation. *J Biol Chem* 1998;**273:**16778-16781.

25. Yeow KM, Kishnani NS, Hutton M*, et al.* Sorsby's fundus dystrophy tissue inhibitor of metalloproteinases-3 (TIMP-3) mutants have unimpaired matrix metalloproteinase

inhibitory activities, but affect cell adhesion to the extracellular matrix. *Matrix Biol* 2002;**21:**75-88.

26. Qi JH, Dai G, Luthert P*, et al.* S156C mutation in tissue inhibitor of metalloproteinases-3 induces increased angiogenesis. *J Biol Chem* 2009;**284:**19927-19936.

27. Lambert V, Wielockx B, Munaut C*, et al.* MMP-2 and MMP-9 synergize in promoting choroidal neovascularization. *FASEB J* 2003;**17:**2290-2292.

28. Chau KY, Sivaprasad S, Patel N*, et al.* Plasma levels of matrix metalloproteinase-2 and -9 (MMP-2 and MMP-9) in age-related macular degeneration. *Eye (Lond)* 2007;**21:**1511-1515.

29. Hussain AA, Lee Y, Zhang J*, et al.* Disturbed Matrix Metalloproteinase Pathway in Both Age-Related Macular Degeneration and Alzheimer's Disease. *J Neurodegener Dis* 2017;**2017:**4810232.

30. Capon MR, Marshall J, Krafft JI*, et al.* Sorsby's fundus dystrophy. A light and electron microscopic study. *Ophthalmology* 1989;**96:**1769-1777.

31. Stone EM, Lotery AJ, Munier FL*, et al.* A single EFEMP1 mutation associated with both Malattia Leventinese and Doyne honeycomb retinal dystrophy. *Nat Genet* 1999;**22:**199-202.

32. Zhang Y, Marmorstein LY. Focus on molecules: fibulin-3 (EFEMP1). *Exp Eye Res* 2010;**90:**374-375.

33. Hulleman JD, Kaushal S, Balch WE*, et al.* Compromised mutant EFEMP1 secretion associated with macular dystrophy remedied by proteostasis network alteration. *Mol Biol Cell* 2011;**22:**4765-4775.

34. Marmorstein LY, Munier FL, Arsenijevic Y*, et al.* Aberrant accumulation of EFEMP1 underlies drusen formation in Malattia Leventinese and age-related macular degeneration. *Proc Natl Acad Sci U S A* 2002;**99:**13067-13072.

35. Stanton JB, Marmorstein AD, Zhang Y*, et al.* Deletion of Efemp1 Is Protective Against the Development of Sub-RPE Deposits in Mouse Eyes. *Invest Ophthalmol Vis Sci* 2017;**58:**1455-1461.

36. Roybal CN, Marmorstein LY, Vander Jagt DL*, et al.* Aberrant accumulation of fibulin-3 in the endoplasmic reticulum leads to activation of the unfolded protein response and VEGF expression. *Invest Ophthalmol Vis Sci* 2005;**46:**3973-3979.

37. Klenotic PA, Munier FL, Marmorstein LY*, et al.* Tissue inhibitor of metalloproteinases-3 (TIMP-3) is a binding partner of epithelial growth factor-containing fibulin-like extracellular matrix protein 1 (EFEMP1). Implications for macular degenerations. *J Biol Chem* 2004;**279:**30469-30473.

38. Fu L, Garland D, Yang Z*, et al.* The R345W mutation in EFEMP1 is pathogenic and causes AMD-like deposits in mice. *Hum Mol Genet* 2007;**16:**2411-2422.

39. Fernandez-Godino R, Bujakowska KM, Pierce EA. Changes in extracellular matrix cause RPE cells to make basal deposits and activate the alternative complement pathway. *Hum Mol Genet* 2018;**27:**147-159.

40. Castelli V, d'Angelo M, Antonosante A*, et al.* Physiology and Pathophysiology of PPARs in the Eye. *Nuclear Receptor Research* 2018;**5:**1-17.

41. Rutar M, Natoli R, Valter K*, et al.* Early focal expression of the chemokine Ccl2 by Müller cells during exposure to damage-inducing bright continuous light. *Invest Ophthalmol Vis Sci* 2011;**52:**2379-2388.

42. Bonyadi M, Jabbarpoor Bonyadi MH, Yaseri M*, et al.* Joint association of complement component 3 and CC-cytokine ligand2 (CCL2) or complement component 3 and CFH polymorphisms in age-related macular degeneration. *Ophthalmic Genet* 2017;**38:**365-370.

43. Sharma NK, Sharma K, Singh R*, et al.* CCL2 single nucleotide polymorphism of rs1024611 implicates prominence of inflammatory cascade by univariate modeling in Indian AMD. *PLoS ONE* 2018;**13:**e0193423.

44. El Khoury J, Toft M, Hickman SE*, et al.* Ccr2 deficiency impairs microglial accumulation and accelerates progression of Alzheimer-like disease. *Nat Med* 2007;**13:**432-438.

45. Qi JH, Ebrahem Q, Moore N*, et al.* A novel function for tissue inhibitor of metalloproteinases-3 (TIMP3): inhibition of angiogenesis by blockage of VEGF binding to VEGF receptor-2. *Nat Med* 2003;**9:**407-415.

46. Qi JH, Ebrahem Q, Ali M*, et al.* Tissue inhibitor of metalloproteinases-3 peptides inhibit angiogenesis and choroidal neovascularization in mice. *PLoS ONE* 2013;**8:**e55667.

47. Fogarasi M, Janssen A, Weber BHF*, et al.* Molecular dissection of TIMP3 mutation S156C associated with Sorsby fundus dystrophy. *Matrix Biol* 2008;**27:**381-392.

48. Chen Y, Brown NJ, Jones R*, et al.* A peptide derived from TIMP-3 inhibits multiple angiogenic growth factor receptors and tumour growth and inflammatory arthritis in mice. *Angiogenesis* 2014;**17:**207-219.

49. Calejo MT, Saari J, Vuorenpää H*, et al.* Co-culture of human induced pluripotent stem cell-derived retinal pigment epithelial cells and endothelial cells on double collagen-coated honeycomb films. *Acta Biomater* 2019;**101:**327-343.

50. Song MJ, Bharti K. Looking into the future: Using induced pluripotent stem cells to build two and three dimensional ocular tissue for cell therapy and disease modeling. *Brain Res* 2016;**1638:**2-14.

51. Hongisto H, Ilmarinen T, Vattulainen M*, et al.* Xeno- and feeder-free differentiation of human pluripotent stem cells to two distinct ocular epithelial cell types using simple modifications of one method. *Stem Cell Res Ther* 2017;**8:**291.

52. Hakala H, Rajala K, Ojala M*, et al.* Comparison of biomaterials and extracellular matrices as a culture platform for multiple, independently derived human embryonic stem cell lines. *Tissue Eng Part A* 2009;**15:**1775-1785.

53. Zhang WY, de Almeida PE, Wu JC. Teratoma formation: A tool for monitoring pluripotency in stem cell research In *StemBook [Internet]*. Harvard Stem Cell Institute: Cambridge (MA), 2012. Available from: https://www.ncbi.nlm.nih.gov/books/NBK133287/

54. Livak KJ, Schmittgen TD. Analysis of relative gene expression data using real-time quantitative PCR and the 2(-Delta Delta C(T)) Method. *Methods* 2001;**25:**402-408.

55. Huang DW, Sherman BT, Lempicki RA. Systematic and integrative analysis of large gene lists using DAVID bioinformatics resources. *Nature Protocols* 2009;**4:**44-57.

56. Huang DW, Sherman BT, Lempicki RA. Bioinformatics enrichment tools: paths toward the comprehensive functional analysis of large gene lists. *Nucleic Acids Research* 2009;**37:**1-13.

57. Bates D, Machler M, Bolker B, *et al.* Fitting linear mixed-effects models using lme4. J Statist Software 2015;**67:**1–48.

References [51-57] are cited only in the supplementary material.

Table 1. Human iPSC lines and characteristics.

Cell line formal name	Status	TIMP3 status	Age when sampled (yr)	Clone	Karyotype	hiPSC markers	Pluripotency	Presence of viral vectors	RPE
RD01*	SFD	p.Ser204Cys	39	RD01A	46, XX t(X;4)(p11;p15)	Pos	EB	Neg	Yes^
				RD01C	46, XX	Pos	EB	Neg	Yes^
RD03	SFD	p.Ser204Cys	48	RD03A	46, XX	Pos	EB Teratomas	Neg	Yes^
				RD03B	46, XX t(2;4)(p23;p1?2)	Pos	EB Teratomas	Neg	Yes^
RD04*	SFD	p.Ser204Cys	42	RD04A	46, XX	Pos	EB Teratomas	Neg	Yes^
				RD04B	46, XX	Pos	EB	Neg	No
Control1 RD08**	Healthy		70		46, XX	Pos	EB	Neg	Yes^^
Control2 UTA.04311.WTs	Healthy		46		46, XX	Pos	EB	Neg	Yes^^
Control3 10211.EURCCs	Healthy		58		46, XX	Pos	EB	Neg	Yes^^

* Siblings; ** unaffected mother of the two siblings. Abbreviations: SFD Sorsby Fundus Dystrophy; p, passage; Pos, positive; EB, embryoid body; Neg, negative; ^n=5 for SFD-hiPSC-RPE, ^^n=3 for control-hiPSC-RPE

Table and figure legends

Figure 1. Retinal fundoscopy and optical coherent tomogram (OCT) images of SFD patient RD04 over a 11-year period. (A) Retinal fundus image showing early choroidal neovascularization (CNV) superior to the fovea* and normal subfoveal OCT (B) Retinal and OCT images of left eye in 2020 showing progression to disciform scar formation and macular scarring due to progression of CNV. (C) OCT image of right eye in 2009 showing disciform scar and abnormal macula. (D) OCT image of right eye in 2020 showing increase in scar size due to ongoing CNV. Progressive macular scarring occurred in each eye despite repeated therapy with bilateral intravitreal bevacizumab over the 11-year period.

Figure 2. Human iPSC-RPE showed characteristic RPE phenotype. (A) Study outline and timetable for cell culture as well as main analyses shown. mo=months, p=passage. (B) Differential interference contrast (DIC) images of the hiPSC-RPE monolayers showing morphology and mosaic pigmentation pattern for the three control lines and the three karyotypically normal SFD lines. Scale bar 20 µm, valid for all images. (C) Scatter dot plots for TEER values measured from separate inserts for each cell line, mean value shown by line and presented above of each dataset, n=separate differentiation experiments. Box blots showing average TEER values for control and SFD-hiPSC-RPE. Whiskers for min and max values with line for median. Mean shown with +. (D) x–y maximum intensity projections (MIP) of confocal z-stacks shown for ZO1 IF labelling. Scale bar 10 µm valid for all images. (E) Confocal z-stack images 4 h after feeding porcine POS and IF labelling with anti-rhodopsin. White arrows indicate internalized POS (green). Phalloidin detected to visualize cells. Scale bar 10 µm, valid for all images. (F) Bar chart showing quantification of average number of POS/frame,

n= number of cell lines with three replicate confocal frames (20x magnification) each. Error bars indicate SD. G) Ratio of apical to basolateral secretion of PEDF. Each dot represents the ratio measured from one insert of a single differentiation experiment. Box plots combining the data for control and SFD. Red line at y=1 indicates equal secretion to both apical and basal sides. The secreted concentrations are presented in supplementary material Figure S6.

Figure 3. RPE ultrastructure analyses by TEM. (A) Cultured hiPSC-RPE from SFD and control patients exhibited characteristic RPE structures. No significant differences were observed between SFD and control hiPSC-RPE cells with regards to (B) cell height (C) apical microvilli length, (D,E) basal laminar area, (F,G) the number of sub-RPE FLS collagen deposits (arrow) per cell and (H,I) the number of melanosomes (open arrow) per cell. Scale bar 2 µm.

Figure 4. TIMP3 expression, secretion, and functionality. (A) RT-qPCR assessment of *TIMP3* transcript levels for all of the hiPSC-RPE lines, individually and combined, to compare expression between control and disease lines. Dots represent technical replicates. Mean fold-change is shown on a logarithmic scale. Dotted lines mark two-fold difference in expression; n=number of cell lines with 3 technical replicates for each. RD08A control set equal to one. (B) A representative image of WB analysis for TIMP3 protein expression showing accumulation of the (21 kDa/24 kDa) monomer, expression of the glycosylated form (27 kDa), and the dimer (48 kDa) in the SFD-hiPSC-RPE. Relative expression levels were measured densitometrically, normalized to β-actin. Error bars show SD, *p=0.0357. (C) Box plots for TIMP3 secretion analysed in CM using ELISA. Median value indicated with a line. (D) EnzCheck collagenase assay assessing the effect of the p.(Ser204Cys) mutant on TIMP3's ability to inhibit MMPs. The general MMP inhibitor 1,10-phenanthroline (+inhibitor) or CM from hiPSC-RPE

containing 50 ng TIMP3, showed a decrease in fluorescence relative to no inhibitor, indicating MMP inhibition. Error bars show SD.

Figure 5. Proteomic profiling revealed upregulation of angiogenesis related pathways and downstream regulators in SFD-hiPSC-RPE comparing to controls. (A) Enriched *diseases and biological functions* for the significantly ($p<0.05$) differentially expressed proteins according to IPA pathway analysis. Heat map displays the general terms (excluding cancer-related terms), which have either highly increased >1.5 (red) or decreased <-1.5 (green) activation z-score. On the left, more specific terms and on the right, the terms are grouped under more general categories. (B) Selected upstream regulators of the enriched pathways and associated proteins with increased (red) and decreased (green) expression, as well as predicted effect of the regulator to protein expression. TGFβ and TNF, known positive regulators of angiogenesis, and negative regulator PPARG and their interactions to protein expression are shown.

Figure 6. Secretion of angiogenesis related proteins. (A) Basal VEGF secretion levels measured by ELISA for control-hiPSC-RPE (n=3 cell lines, 5 inserts each) and SFD-hiPSC-RPE (n=5 cell lines, 3-4 inserts each). (B) Human Angiogenesis Array membranes showing basal secretion of 15 angiogenesis-related proteins and (C) densitometric relative quantification of the spot intensities for SFD-hiPSC-RPE compared to control.

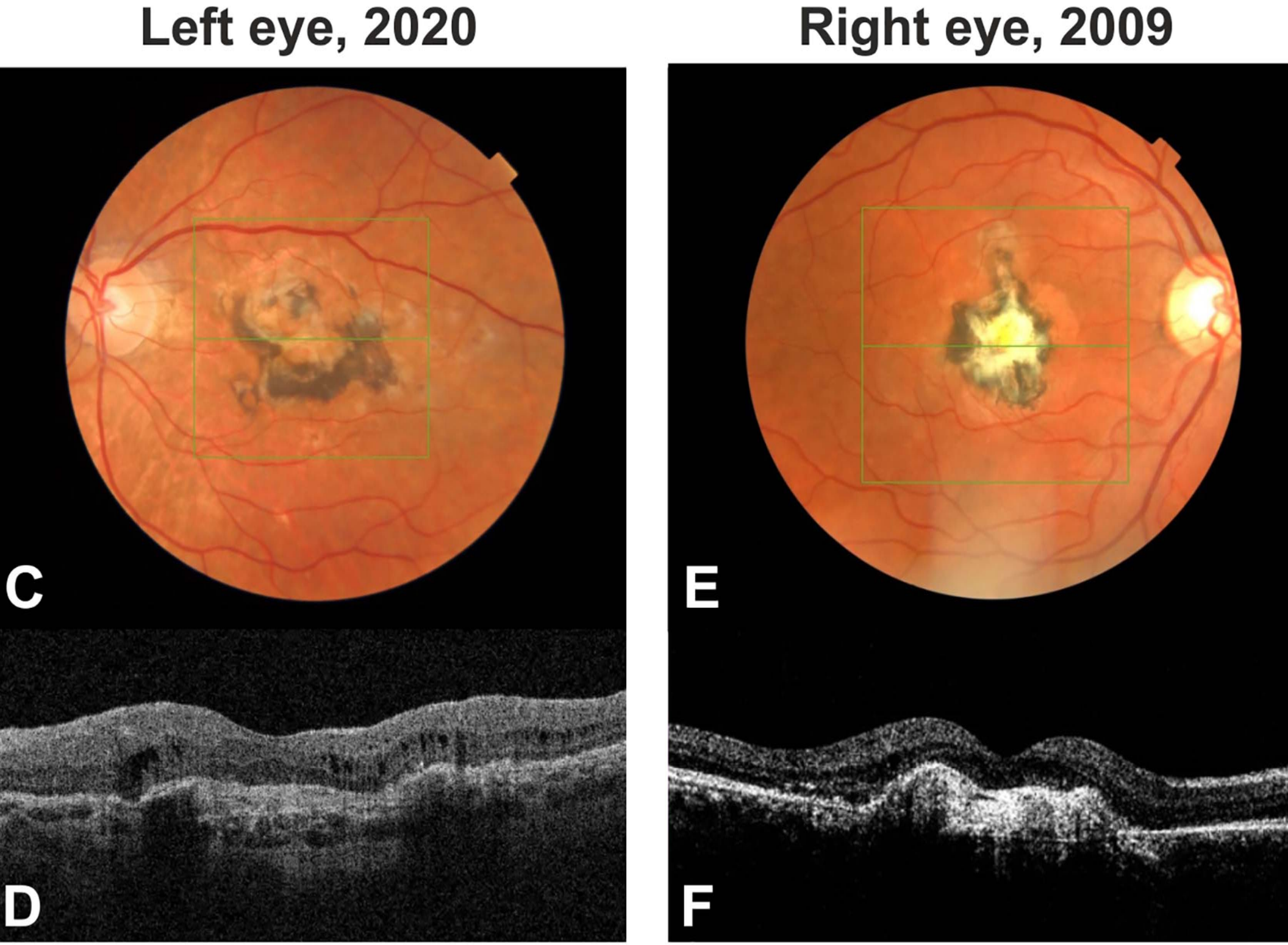
Left eye, 2020
Right eye, 2009
C
D
E
F

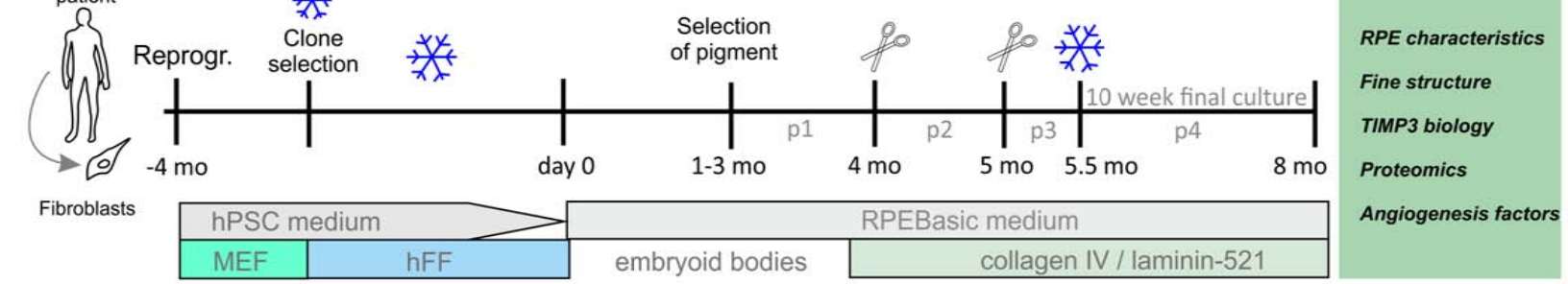
Reprogr.
Clone selection
Selection of pigment
10 week final culture
p1
p2
p3
p4
-4 mo
day 0
1-3 mo
4 mo
5 mo
5.5 mo
8 mo
Fibroblasts
hPSC medium
MEF
hFF
embryoid bodies
RPEBasic medium
collagen IV / laminin-521
RPE characteristics
Fine structure
TIMP3 biology
Proteomics
Angiogenesis factors

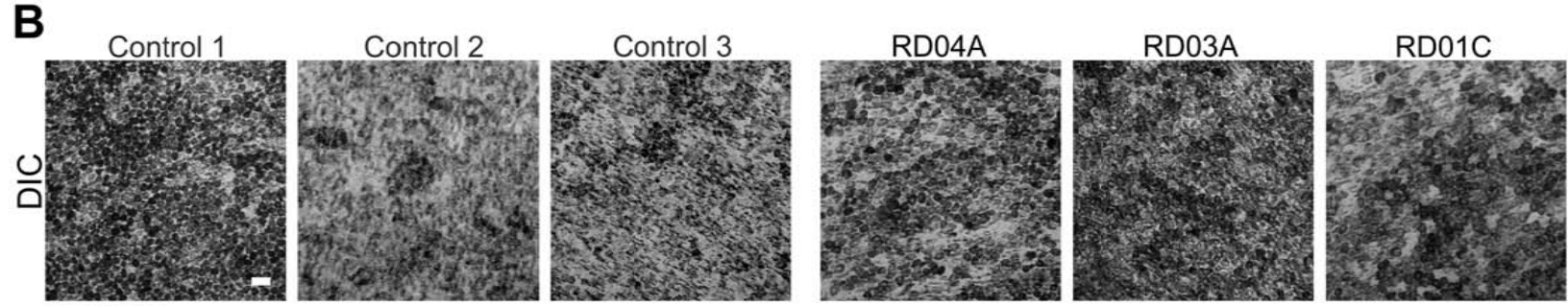
B
Control 1
Control 2
Control 3
RD04A
RD03A
RD01C
DIC

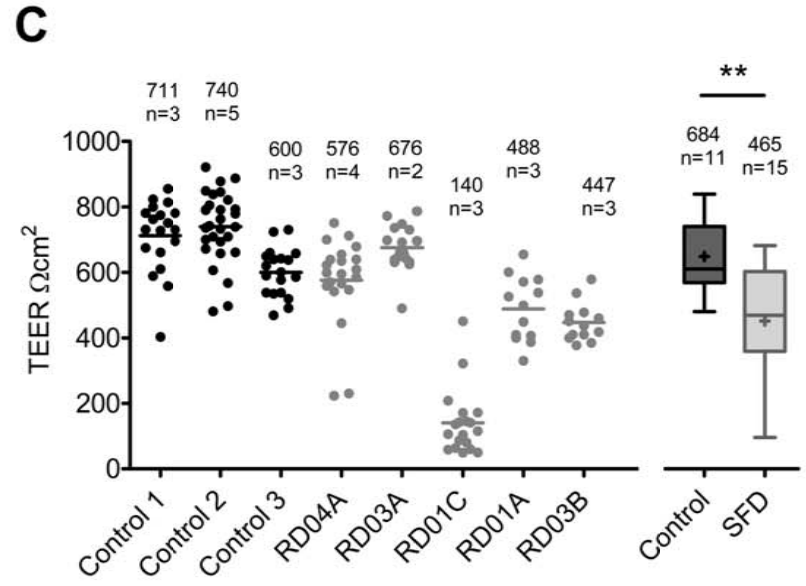
C
TEER Ωcm2
711 n=3
740 n=5
600 n=3
576 n=4
676 n=2
140 n=3
488 n=3
447 n=3
684 n=11
465 n=15
**
Control 1
Control 2
Control 3
RD04A
RD03A
RD01C
RD01A
RD03B
Control
SFD

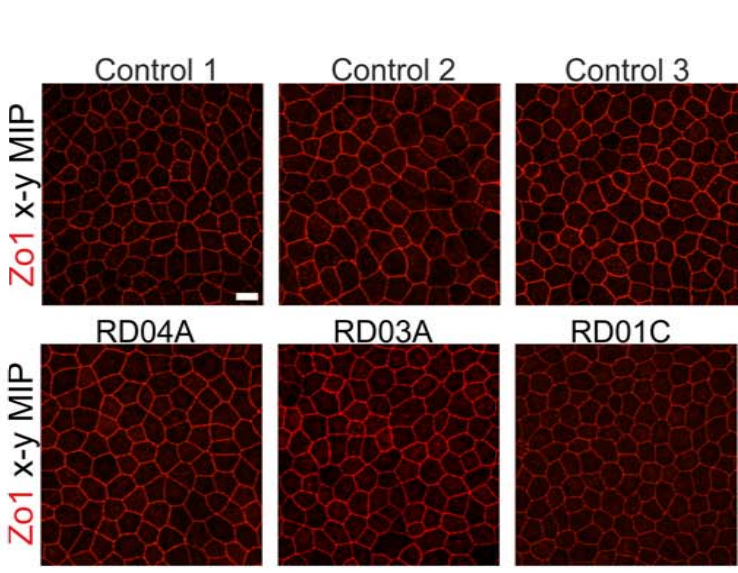
D
Control 1
Control 2
Control 3
Zo1 x-y MIP
RD04A
RD03A
RD01C
Zo1 x-y MIP

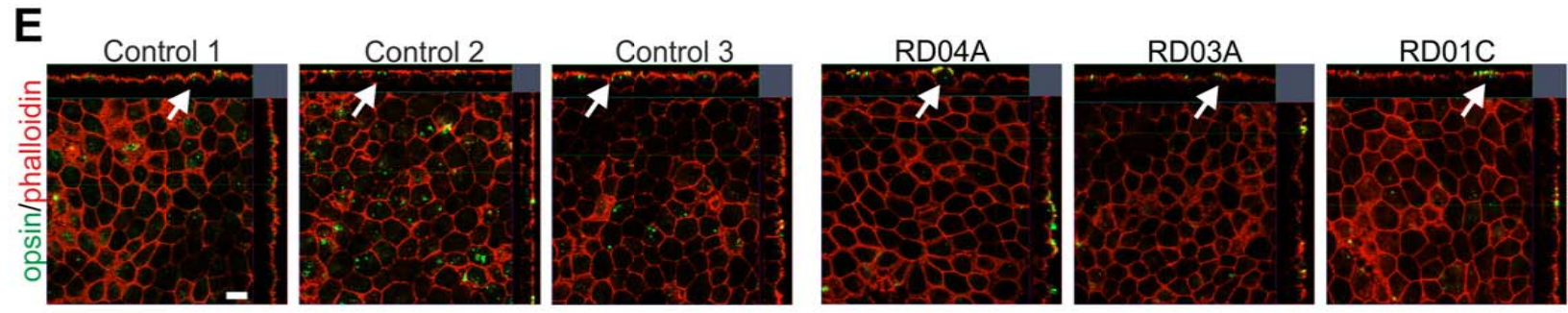
E
Control 1
Control 2
Control 3
RD04A
RD03A
RD01C
opsin/phalloidin

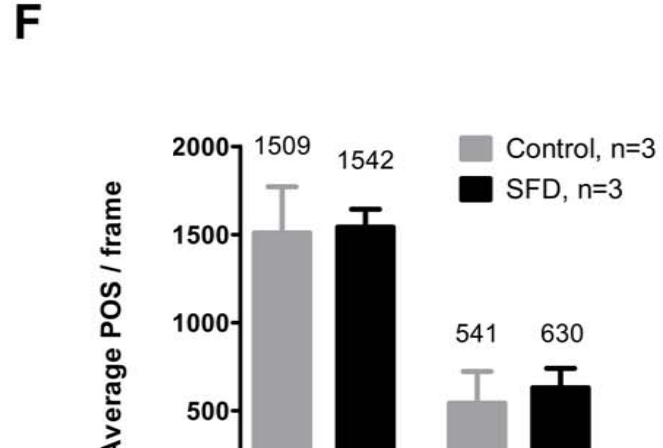
F
Average POS / frame
1509
1542
541
630
Control, n=3
SFD, n=3

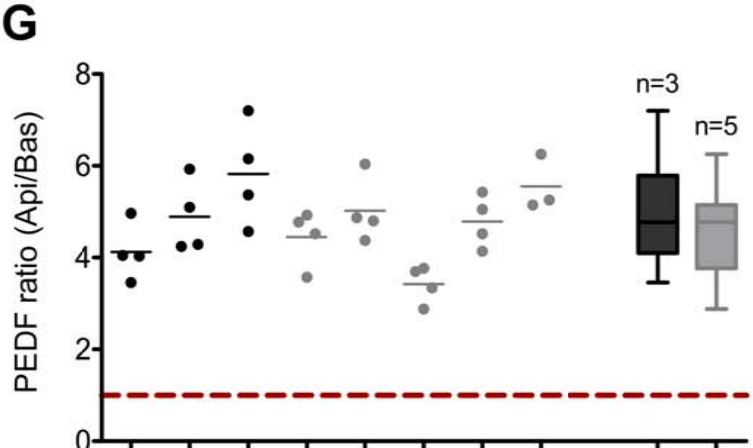
G
PEDF ratio (Api/Bas)
n=3
n=5

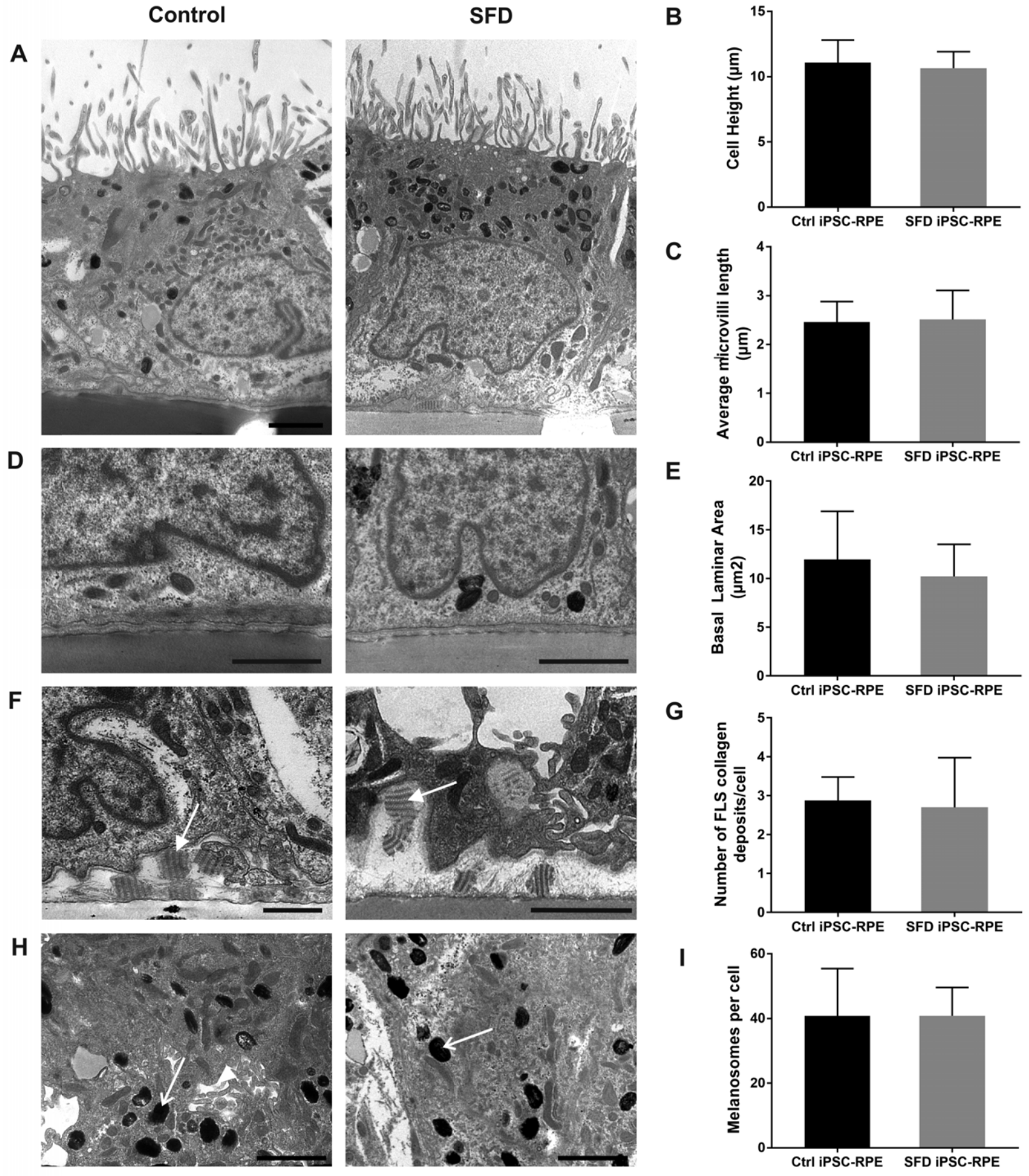
Control
SFD
A
B
Cell Height (µm)
15
10
5
0
Ctrl iPSC-RPE
SFD iPSC-RPE
C
Average microvilli length (µm)
4
3
2
1
0
Ctrl iPSC-RPE
SFD iPSC-RPE
D
E
Basal Laminar Area (µm2)
20
15
10
5
0
Ctrl iPSC-RPE
SFD iPSC-RPE
F
G
Number of FLS collagen deposits/cell
5
4
3
2
1
0
Ctrl iPSC-RPE
SFD iPSC-RPE
H
I
Melanosomes per cell
60
40
20
0
Ctrl iPSC-RPE
SFD iPSC-RPE

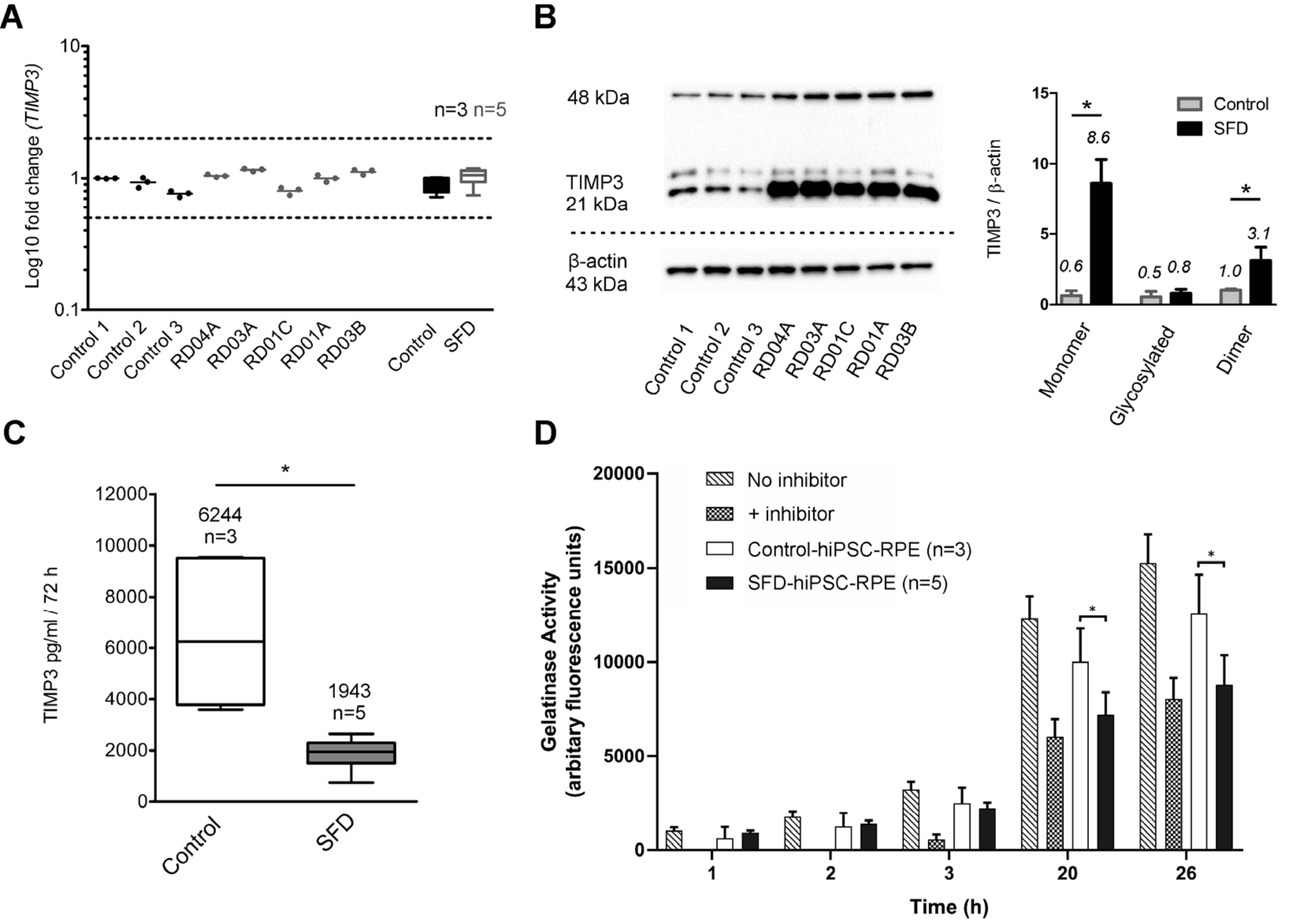
A
Log10 fold change (TIMP3)
10
1
0.1
n=3 n=5
Control 1
Control 2
Control 3
RD04A
RD03A
RD01C
RD01A
RD03B
Control
SFD
B
48 kDa
TIMP3
21 kDa
β-actin
43 kDa
Control 1
Control 2
Control 3
RD04A
RD03A
RD01C
RD01A
RD03B
TIMP3 / β-actin
15
10
5
0
Control
SFD
*
8.6
*
3.1
0.6
0.5
0.8
1.0
Monomer
Glycosylated
Dimer
C
TIMP3 pg/ml / 72 h
12000
10000
8000
6000
4000
2000
0
*
6244
n=3
1943
n=5
Control
SFD
D
Gelatinase Activity
(arbitary fluorescence units)
20000
15000
10000
5000
0
No inhibitor
+ inhibitor
Control-hiPSC-RPE (n=3)
SFD-hiPSC-RPE (n=5)
*
*
1
2
3
20
26
Time (h)

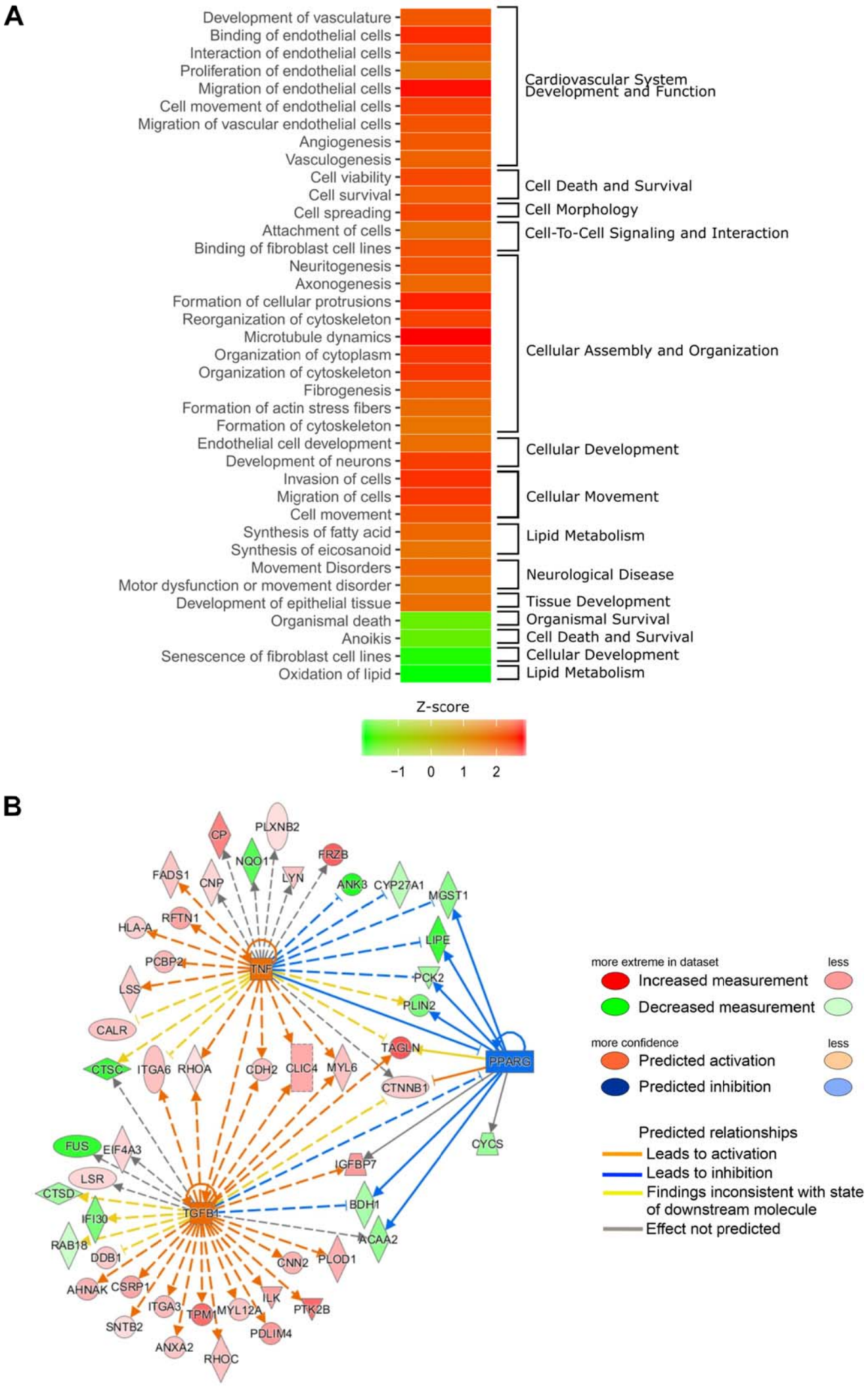
A
Development of vasculature
Binding of endothelial cells
Interaction of endothelial cells
Proliferation of endothelial cells
Migration of endothelial cells
Cell movement of endothelial cells
Migration of vascular endothelial cells
Angiogenesis
Vasculogenesis
Cell viability
Cell survival
Cell spreading
Attachment of cells
Binding of fibroblast cell lines
Neuritogenesis
Axonogenesis
Formation of cellular protrusions
Reorganization of cytoskeleton
Microtubule dynamics
Organization of cytoplasm
Organization of cytoskeleton
Fibrogenesis
Formation of actin stress fibers
Formation of cytoskeleton
Endothelial cell development
Development of neurons
Invasion of cells
Migration of cells
Cell movement
Synthesis of fatty acid
Synthesis of eicosanoid
Movement Disorders
Motor dysfunction or movement disorder
Development of epithelial tissue
Organismal death
Anoikis
Senescence of fibroblast cell lines
Oxidation of lipid
Cardiovascular System Development and Function
Cell Death and Survival
Cell Morphology
Cell-To-Cell Signaling and Interaction
Cellular Assembly and Organization
Cellular Development
Cellular Movement
Lipid Metabolism
Neurological Disease
Tissue Development
Organismal Survival
Cell Death and Survival
Cellular Development
Lipid Metabolism
Z-score
−1
0
1
2
B
PLXNB2
CP
NQO1
FRZB
FADS1
CNP
LYN
ANK3
CYP27A1
MGST1
RFTN1
HLA-A
LIPE
PCBP2
TNF
PCK2
LSS
PLIN2
CALR
TAGLN
CTSC
ITGA6
RHOA
CDH2
CLIC4
MYL6
PPARG
CTNNB1
CYCS
FUS
EIF4A3
IGFBP7
LSR
CTSD
BDH1
TGFB1
IFI30
ACAA2
RAB18
DDB1
CNN2
PLOD1
AHNAK
CSRP1
ILK
ITGA3
TPM1
MYL12A
PTK2B
SNTB2
PDLIM4
ANXA2
RHOC
more extreme in dataset
less
Increased measurement
Decreased measurement
more confidence
less
Predicted activation
Predicted inhibition
Predicted relationships
Leads to activation
Leads to inhibition
Findings inconsistent with state of downstream molecule
Effect not predicted

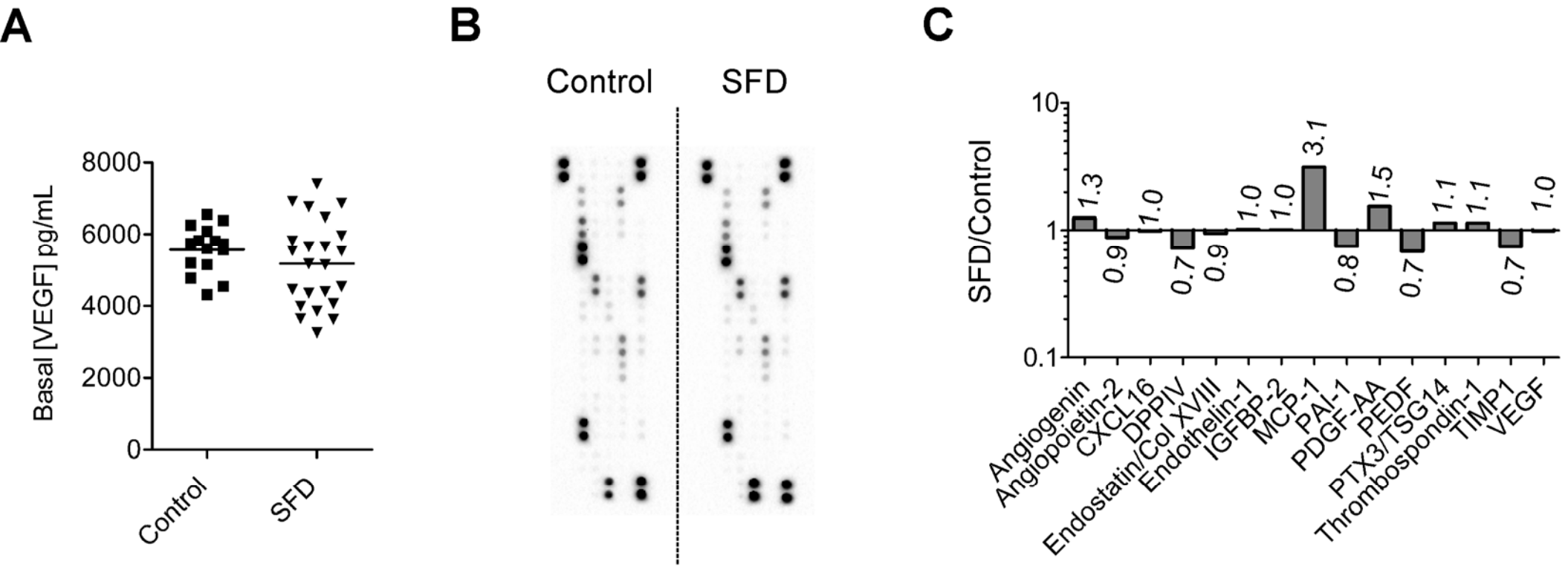
A
Basal [VEGF] pg/mL
8000
6000
4000
2000
0
Control
SFD
B
Control
SFD
C
SFD/Control
10
1
0.1
1.3
0.9
1.0
0.7
0.9
1.0
1.0
3.1
0.8
1.5
0.7
1.1
1.1
0.7
1.0
Angiogenin
Angiopoietin-2
CXCL16
DPPIV
Endostatin/Col XVIII
Endothelin-1
IGFBP-2
MCP-1
PAI-1
PDGF-AA
PEDF
PTX3/TSG14
Thrombospondin-1
TIMP1
VEGF

In-vitro stem cell modelling demonstrates a proof-of-concept for excess functional mutant TIMP3 as the cause of Sorsby Fundus Dystrophy

H Hongisto, JM Dewing *et al. J Pathol* DOI: 10.1002/path.

Supplementary materials and methods

Reference numbers refer to the main text list

Human iPSC establishment and characterization

Fibroblasts isolated from patient skin biopsies were cultured in DMEM with high glucose supplemented with 10% FBS, 2 mM glutamine, and 100 U/mL penicillin/streptomycin (Thermo Fisher Scientific, Waltham, MA, USA). The isolated human fibroblasts were reprogrammed into human iPSCs using CytoTune-iPS Sendai Reprogramming kit (Thermo Fisher Scientific) on mouse embryonic fibroblast (MEF) feeder cells according to the manufacturer's instructions. All hiPSC lines were transferred to, and cultured on, mitotically inactivated human foreskin fibroblast feeder cells (hFF, CRL-2429, ATCC, Manassas, VA, USA) in standard hPSC culture medium: ko-DMEM supplemented with 20% KnockOut™ Serum Replacement (KO-SR), 2 mM GlutaMAX™ Supplement, 0.1 mM 2-mercaptoethanol (all from Thermo Fisher Scientific), 1% MEM Non-Essential Amino Acids Solution, 50 U/ml Penicillin-Streptomycin (both from Lonza, Basel, Switzerland), and 8 ng/ml human basic fibroblast growth factor (bFGF, Peprotech, Cranbury, USA). Culture medium was replaced 5 times each week and undifferentiated colonies manually passaged to fresh feeder cell layers weekly. Feeder-free culture was done as previously described in [51]. Prior to RPE differentiations, the hiPSCs were thoroughly characterized (Table 1) and tested mycoplasma negative (not shown).

Human iPSC immunofluorescence labelling

Human iPSC immunofluorescence (IF) labelling for pluripotency markers were done as previously described [52]. using the following antibodies: NANOG (1:200, AF1997, R&D Systems, Minneapolis, Canada), OCT-3/4 (1:200, AF1759, R&D Systems), SSEA-3 (1:600, MAB1434, R&D Systems), SSEA-4 (1:200, MAB1435, R&D Systems), TRA-1-60 (1:200, MAB4360, Merck Millipore, Darmstad, Germany), TRA-1-81 (1:200, SC-21706, Santa Cruz Biotechnology, Dallas, Texas, USA). Nuclei were counterstained with 4´, 6´ diamidino-2-phenylidole (DAPI) included in the VECTASHIELD™ Mounting Medium (Vector Laboratories Inc., Burlingame, CA, USA). Images were acquired using an Olympus IX51 phase contrast microscope with fluorescence optics and a Olympus DP30BW camera (Olympus Corporation, Tokyo, Japan).

EB differentiation for* in vitro *pluripotency

Human iPSC pluripotency was verified by observing spontaneous differentiation as EBs, followed by immunofluorescence labelling for derivative cells of the three embryonic germ layers. Undifferentiated hiPSC colonies were manually cut to embryoid bodies and differentiated in suspension for 1–2 weeks in EB-medium: KnockOut™ DMEM supplemented with 10% fetal bovine serum (FBS), 2 mM GlutaMAX™ Supplement, 0.1 mM 2-mercaptoethanol, 1% MEM Non-Essential Amino Acids Solution, and 50 U/ml Penicillin-Streptomycin (all from Thermo Fisher Scientific). Thereafter the EBs were plated onto 0.5 µg/cm^2 human recombinant laminin-521 (Biolamina, Stockholm, Sweden) coated 48-wp culture plates and cultured for 7 d. The cells were then washed, fixed with 4% paraformaldehyde and labelled similarly to undifferentiated hPSCs. Following primary antibodies were used: alpha-smooth muscle actin (α-SMA, 1:400, MAB1420, R&D Systems) for mesoderm, alpha-fetoprotein (AFP, 1:200, MAB1369, R&D Systems) or SOX17 (1:200, AF1924, R&D Systems) for endoderm, and OTX2 (1:200, AF1979,

R&D Systems) for ectoderm. EBs were mounted with VECTASHIELD™ Mounting Medium including DAPI and images were acquired using an Olympus IX51 microscope.

Teratomas for in vivo *pluripotency*

Human iPSC pluripotency was confirmed for three of the clones (RD04A, RD03A, and RD03B) *in vivo* with a teratoma assay. Teratomas were formed after injection of hiPSCs into immunocompromised (SCID) mice and the tissue processed for immunohistochemical and H&E staining as described by Zhang *et al* [53]. hiPSC-derived teratomas were stained with antibodies against synaptophysin and OTX2 (ectoderm/neuroectoderm); alpha-SMA (mesoderm) and AFP (endoderm).

Karyotyping

To examine chromosomal integrity, the hiPSCs were karyotyped using either Giemsa banding at Wessex Regional Genetics Laboratory, Salisbury District Hospital, Salisbury, UK, or a KaryoLite BoBs assay (Perkin Elmer) at the Finnish Microarray and Sequencing Centre (FMSC), Turku Centre for Biotechnology, Turku, Finland. For G-banding, a minimum of 10 cells (metaphases) were studied.

TIMP3 *sequencing*

Genomic DNA from hiPSCs was isolated and the *TIMP3* region of interest was sequenced by SourceBioscience (Nottingham, UK) using the following primers: F: ACCGACATGCTCTCCAATTT; R: AGTGTCCAAGGGAAGCTCAG.

RT-qPCR to confirm removal of viral vectors

Removal of Sendai virus and transgenes from the hiPSC clones was confirmed using RT-qPCR using Taqman Assays with primers and probes specific for Sendai-delivered exogenous transcription factors and not detecting the corresponding endogenous factors. RT-qPCR was performed as described for *TIMP3* expression analysis using

following TaqMan Gene Expression Assays: SEV (Mr04269880_mr), SEV-KOS (Mr04421257_mr), SEV-CMYC (Mr04269876_mr), SEV-KLF4 (Mr04421256_mr), and GAPDH (HS99999905_m1) (All from Thermo Fisher Scientific).

RPE differentiation

For RPE differentiation, hiPSC on hFF feeders were cut to embryoid bodies and differentiated in suspension in RPEbasic medium (as hPSC medium but with 15% KO-SR and no bFGF) until sufficient pigmentation was achieved (1–3 months). Pigmented foci were manually cut off and further dissociated with TrypLE™ Select Enzyme (Thermo Fisher Scientific), then plated for expansion on 5 µg/cm^2 human placental collagen type IV (col IV; C5533, Sigma-Aldrich, St. Louis, MO, USA) coated culture plates for approximately four weeks (RPE passage 1). RPE cells were then passaged twice using TrypLE™ Select Enzyme and reseeded in 1:2–1:4 ratio for purification and expansion (RPE passages 2–3). Cells were cryopreserved at passage 3 in RPEbasic supplemented with 40% KO-SR and 10% dimethyl sulfoxide (DMSO; Sigma-Aldrich). For the final RPE passage 4, the cells were passaged or thawed in permeable Millicell 24-well polyethylene terephthalate (PET) hanging cell culture inserts with pore size of 1.0 µm (Merck Millipore) or 24-well plates coated with 0.75–1.8 µg/cm^2 human recombinant laminin-521 (Biolamina) and/or 5–10 µg/cm2 col IV.

RPE characterization

IF labelling

For IF labelling, the hiPSC-RPE cells cultured for 70 d on permeable cell culture inserts were washed three times with DPBS (Lonza) and fixed for 15 min with 4%

paraformaldehyde (pH 7.4, Sigma-Aldrich) at room temperature (RT) following repeated washings with DPBS. The cells were permeabilised with 0.1% Triton X-100 in DPBS (Sigma-Aldrich) at RT for 15 min. Unspecific binding sites were blocked with 3% BSA in DPBS (BSA; Sigma-Aldrich) at RT for 1 h. Samples were incubated with primary antibodies diluted in 3% BSA overnight at +4 °C. Following antibodies were used: CRALBP (1:200, ab15051, Abcam Cambridge, UK), ZO-1 (1:200, 61-7300, Thermo Fisher Scientific), alpha 1 sodium potassium ATPase (1:200, ab7671, Abcam), and MERTK (1:50, H00010461-M01, Abnova, Taipei, Taiwan), ezrin (1:200, PAB7060, Abnova), ARL13b (1:1000, 17711-1-AP, Proteintech, Rosemont, USA). The cells were washed three times with DPBS and labelled with secondary antibodies (1:200 in 3% BSA) for 1 h at RT: Alexa Fluor 568-conjugated donkey anti-rabbit IgG (A10042) and donkey anti-goat IgG (A-11057), and Alexa Fluor 488-conjugated donkey anti-mouse IgG (A-21202) and donkey anti-rabbit IgG (A-21206, all from Thermo Fisher Scientific). Phalloidin-tetramethylrhodamine B isothiocyanate (1:1000, P1951, Sigma-Aldrich) was used for labelling filamentous actin. Cells were washed three times with DPBS and nuclei were counterstained with DAPI present in ProLong® Gold Antifade Mountant with DAPI (P36931, Thermo Fisher Scientific). Alternatively, cells were counterstained with Hoechst (1:3000 in DBPS, 33342, Thermo Fisher Scientific) followed by mounting. Images were captured using a Zeiss LSM 800 LSCM confocal microscope (Carl Zeiss Microscopy GmbH, Jena, Germany) using a 40x objective or 63× oil immersion objective.

Transepithelial Electrical Resistance

Transepithelial electrical resistance (TEER) was measured with a Millicell electrical resistance system volt-ohm meter (Merck Millipore) from cell culture inserts without balancing to RT before measuring. TEER values (Ω^*cm^2) were calculated by subtracting

the TEER value of empty inserts in culture medium and by multiplying with the surface area of the insert (0.3 cm^2).

In Vitro *phagocytosis assay*

The functional capacity of the hiPSC-RPE to phagocytose porcine photoreceptor outer segments (POS) was assessed *in vitro*. Porcine POS were isolated from porcine eyes immediately after slaughter, collected to cold AMES' medium (Sigma-Aldrich) supplemented with 0.5% Penicillin-Streptomycin and kept on ice, protected from light, until POS extraction approximately 2 h later. The retinas were removed using scissors, blades, and tweezers in a dark room under red light. Retinas were homogenized with gentle shaking in 0.73 M sucrose phosphate buffer, filtered twice through a gauze and cell types separated in sucrose gradient (0.75 M, 1.0 M, 1.25 M, 1.5 M, 1.75 M) by ultracentrifugation (Optima ultracentrifuge, Beckman Coulter, Inc., Brea, CA, USA) at 112,400 x *g* for 48 min at +4 °C. The faint pink POS layer was collected in phosphate buffer, washed twice with centrifugation at 3000 x *g* for 10 min at +4 °C, and stored as aliquots in 73 mM sucrose phosphate buffer at –80 °C. For the phagocytosis assay, POS were defrosted, centrifuged 2700 x *g*, 4 min (Eppendorf Centrifuge 5415 R, Merck Millipore) washed with DPBS, centrifuged again, and suspended in medium containing 10% FBS (Thermo Fisher Scientific). An equal quantity of POS suspension was added to the apical side of the hiPSC-RPE inserts and incubated for 4 h at 37 °C in the dark. The inserts were washed several times with DPBS and fixed with 4% PFA for 15 min at RT followed by DPBS washes. Cells were permeabilized, blocked and immunolabelled as described above with monoclonal anti-opsin primary antibody (1:200, 04886 Sigma-Aldrich). Z-stacks were captured using a Zeiss LSM 800 LSCM confocal microscope with 63× oil immersion objective. For quantification of attached (total) and internalised POS, three z-stacks for each hiPSC-RPE line were taken at 20 x magnification and 0.1 µm

interval. The numbers of POS were quantified using ImageJ Image Processing and Analysis software (ImageJ, https://imagej.nih.gov/ij/).

ELISA

Secretion of PEDF, VEGF, and TIMP3 by the hiPSC-RPE was studied using ELISA. Apical (400 µl) and basal (800 µl) culture medium of several replicate cell culture inserts (cells 70 d at final RPE passage 4) were collected after 72 h incubation. 2 ml of medium was collected from 24-well plate wells (cells 84 d at final RPE passage 4) after 72 h incubation. The samples were stored at –80 °C until analysed using a Human Serpin F1/PEDF DuoSet ELISA kit (DY1177-05, R&D Systems) and 1:10,000 dilution of apical medium (1:5,000 dilution for basal medium). DuoSet ELISA Ancillary Reagent Kit 2 (DY008, R&D Systems) was used for accessory reagents as instructed by the manufacturer. TIMP3 secretion was measured using a Human TIMP3 ELISA Kit (MIG-5) (ab119608, Abcam) with 1:2 dilutions according to the manufacturer's instructions. VEGF was measured using a Human VEGF Quantikine ELISA Kit (DVE00, R&D Systems) and basal medum at 1:15 dilution according to manufacturer's instructions. Medium samples incubated without cells were collected for background measurements. Optical densities were measured using a Perkin Elmer Wallac 1420 VICTOR2™ Microplate Reader (Perkin Elmer-Wallace, Norton, OH, USA). Standard curves were created, and concentrations calculated using the parameter logistic (4PL) curve fit of MyAssays analysis software (www.myassays.com).

***TIMP3* RT-qPCR**

Relative *TIMP3* transcript level between control and SFD-hiPSC-RPE was analysed by RT-qPCR. Total RNA was extracted from hiPSC-RPE cultured on 24-well plates for 73 d, using a RNeasy Plus Mini Kit (Qiagen, Redwood City, CA, USA) according to the manufacturer's instructions. RNA concentration and quality were determined using NanoDrop-2000 spectrophotometer (NanoDrop Technologies, Thermo Fisher Scientific). From each RNA sample, 200 ng were used to synthesize cDNA using a High-Capacity cDNA Reverse Transcription Kit (Thermo Fisher Scientific). The resulting cDNA samples were analysed by qPCR using TaqMan Gene Expression Assay HS00165949_m1 (Applied Biosystems, Thermo Fisher Scientific). All samples were run as triplicate reactions in a 7300 Real-Time PCR system (Applied Biosystems, Thermo Fisher Scientific). Based on the cycle threshold (CT) values, the relative quantification was calculated by applying the $2^{-\Delta\Delta Ct}$ method [54]. Results were normalized to *GAPDH* (Hs99999905_m1), with the Control 1 (RD08A) set as the calibrator (fold-change equal to 1) to determine the relative quantities of gene expression in each hiPSC-RPE line. The analysis was repeated with similar results from separate differentiation experiment using total RNA extracted from cells cultured for 70 d on inserts.

TEM

For transmission electron microscopy (TEM) analysis the hiPSC-RPE were fixed, dehydrated, and embedded in epoxy resin as described in detail [14]. The samples were sectioned and imaged at the Biomedical Imaging Unit, Southampton General Hospital. Silver/gold ultrathin sections were cut using a Reichert Ultracut E ultramicrotome (Leica Microsystems, Wetzlar, Germany), collected on 200 mesh copper grids, stained with Reynolds' lead stain, and imaged using a Hitachi HT7700 transmission electron

microscope (Fukuoka, Japan). Cellular structures were counted from the TEM images with the help of ImageJ software.

Western blotting

For western blotting (WB), the hiPSC-RPE (n=3 control, n=5 SFD) were cultured on 24-well plates for 70–76 days. Samples were lysed in 2x Laemmli Sample Buffer (Bio-Rad, Hercules, CA, USA) containing 2-mercaptoethanol (Sigma-Aldrich) and separated using 7.5%, 10%, or 12% SDS–polyacrylamide gel electrophoresis. Samples were transferred onto 0.2 µm polyvinylidene fluoride membrane (PVDF) included in the Trans-Blot® Turbo™ RTA Mini PVDF Transfer Kit (Bio-Rad) as instructed by the manufacturer. Blocking was done with 5% milk powder in Tris-buffered saline supplemented with 0.05% Tween 20 (TBST, Sigma-Aldrich) for 1–3 h at RT. The membrane was incubated in primary antibody diluted in 5% milk powder-TBST, overnight at 4 °C. The following primary antibodies were used: Anti-TIMP3 (1:750, ab39184, Abcam), anti-TIMP3 (1:750, ab58804, Abcam), anti-Apolipoprotein E (1:1000, AB947, Merck Millipore), fibulin 3 antibody (1:400, sc-33722, Santa Cruz Biotechnology), and β-Actin antibody (1:1000; sc-47778, Santa Cruz Biotechnology). Thereafter, secondary antibodies: m-IgGk BP-HRP (1:500, sc-516102-CM, Santa Cruz Biotechnology), Swine Anti-Rabbit Immunoglobulins/HRP (1:2000, P0217 Agilent Dako, Santa Clara, CA, USA), and rabbit anti-goat IgG-HRP (1:2000, sc-2922, Santa Cruz Biotechnology) were incubated for 1 h at RT diluted in 5% milk powder-TBST. Protein–antibody complexes were detected using Amersham™ ECL™ Prime Western Blotting Detection Reagent (GE Healthcare, Little Chalfont, UK) and visualized using the Chemi Doc MP System (Bio-Rad). For re-use, the membranes were stripped with 0.1 M 2-mercaptoethanol, 2% w/v SDS, and 62.5 mM Tris-HCl (pH 6.8 at 25°C) in dH_2O for 30 min at 56 °C, followed by immunoblotting and

detection as above. Relative quantitation of band intensities was done with ImageJ software, relative to the β-actin band intensity of the same lane and with the protein/β-actin ratio of Control 1 (RD08A) set equal to 1. The WB analysis for TIMP3 was repeated four times with samples from separate differentiation experiments and twice for the other antibodies.

Collagenase assay

For collagenase assay, hiPSC-RPE (n=3 control, n=5 SFD) were cultured on 24-well plates for 84 d and RPE basic culture media was collected from 24-well plates after 72 h incubation on the cells (2 ml/well) and stored at –80 °C until analysed. An aliquot was set aside for an ELISA assay to quantify TIMP3 concentration in each sample. The MMP inhibitory activity of conditioned medium (CM) was examined using a collagenase activity assay (EnzChek Gelatinase/collagenase kit; Invitrogen) with collagenase type IV from Clostridium histolyticum, as recommended by the manufacturer. In brief, 80 µl of CM containing 50 ng of TIMP3 (as quantified by ELISA) was incubated with 1 mg/ml quenched fluorescein-conjugated DQ gelatin and 0.1 U/ml collagenase at 22 °C and fluorescence was quantified on a microplate reader at multiple time points (1–26 h).

SWATH-MS proteomics

For mass spectrometry, the hiPSC-RPE were cultured for 70 d on 24-well plates. Replicate wells (3–7) were used for each cell line. The cells were washed with DPBS, detached with quick scraping, and pelleted by centrifugation. The cell pellets were frozen at –80 °C until protein extraction, concentration measurement, reduction, alkylation and tryptic digestion as described in detail previously [15,16] Size exclusion filters (10 kDa; Pall Corporation, Port Washington, NY, USA) were used in sample preparation. For MS

analysis, the samples were diluted to the same concentration and 2.7 µg sample was injected into a Eksigent 425 NanoLC coupled with high speed TripleTOF 5600+ mass spectrometer (Ab Sciex, Concord, Canada). Two replicate MS analyses were run for each sample. Analysis of the samples was done as described [15,16]. Sequential window acquisition of all theoretical fragment ion spectra (SWATH) library was created using ProteinPilot software version 4.6 (Sciex, Redwood City, CA, USA). The library was used to analyse MS/MS data and search against the Uniprot reviewed library (Swiss-Prot) for protein identification as described [16]. During data processing, means of replicate MS analysis were taken. Proteins with median coefficient of variation (CV) > 30 were filtered out (approx 30% of proteins), and the remaining 1638 proteins included in the final analysis. Differences in protein expression were compared between SFD and control-iPSC-RPE by comparing the relative fold-change values. The Database for Annotation, Visualization and Integrated Discovery (DAVID) v6.8 [55,56] was used for functional annotation enrichment and clustering of the proteins with fold-change difference ≥1.5, according to gene ontology (GO-term) subontologies: Biological Process, Molecular Function, and Cellular Component. Two-level nested ANOVA model (LMER, linear mixed effects model) was implemented with lme4 package [57] in order to analyse statistical significance in protein expression differences between SFD-hiPSC-RPE and control-hiPSC-RPE, while taking into account the repeated measures from same subjects. For this analysis, the protein expression levels were transformed to log2 scale. A coefficient of the model corresponding to fold-change was given for each protein and $p<0.05$ was considered significant. All statistical analyses for the proteomics data were performed using R software version 3.25.3 (R Core Team, Foundation for Statistical Computing, Vienna, Austria) and IPA software (IPA; Qiagen).

Human Angiogenesis Array

Secretion of angiogenesis related proteins into basal culture media incubated for 72 h on hiPSC-RPE insert cultures was analysed using the Proteome Profiler Human Angiogenesis Array Kit (ARY007, R&D systems) according to manufacturer's instructions. Media from control (n=3 cell lines, 2 inserts each) and SFD (n=5 cell lines, 2 inserts each) were pooled to 1 ml from both control and SFD separately and loaded on separate arrays. Chemiluminescence was visualized using a Chemi Doc MP System (Bio-Rad). The average pixel intensities of the duplicate spots for each protein were analysed using Image Lab Software 5.2 (Bio-Rad). Relative changes for SFD/Control were analysed for each protein from non-saturated spots at linear range of chemiluminescence detection.

Software and statistics

Zen 2.3 SP1 Black (Carl Zeiss Microscopy GmbH, Germany) and Adobe Photoshop CC 20.0.4 (San Jose, CA, USA) software were used for editing confocal images. Box plots and bar charts were generated, and statistics performed using GraphPad Prism version 5.02 for Windows (GraphPad Software, San Diego, CA, USA). Figure panels were assembled using CorelDRAW X7 (Corel Corporation, Ottawa ON, Canada). Microsoft Excel (Redmond, WA, USA) was used for data processing.

In-vitro stem cell modelling demonstrates a proof-of-concept for excess functional mutant *TIMP3* as the cause of Sorsby Fundus Dystrophy

H Hongisto, JM Dewing *et al. J Pathol* DOI: 10.1002/path

Supplementary figures S1–S11

Figure S1. SFD-hiPSC characteristics. Representative images for RD04A shown in (A-D). (A) Phase contrast (PC) images showing typical colony morphology on human foreskin fibroblast feeder cells (left) and in feeder-free culture conditions (right), and immunofluorescence images of hiPSC colonies showing expression of pluripotency markers NANOG, octamer-binding transcription factor-3/4 (OCT-3/4), stage-specific embryonic antigen-3 and -4 (SSEA-3/SSEA-4), tumour-related Antigen-1-60 and -1-81 (TRA-1-60/TRA-1-81). (B) Expression of embryonic germ layer markers after EB differentiation *in vitro*: orthodenticle Homeobox 2 (OTX2), alpha-fetoprotein (AFP), and alpha-smooth muscle actin (alpha-SMA). DAPI to counterstain nuclei. Scale bar 200 µm, valid for all images. (C) Expression of the corresponding germ layer markers in immunohistochemical staining of teratomas induced by hiPSC injection to SCID mice. Scale bar 100 µm, valid for all images. (D) Normal, diploid karyogram after Giemsa staining. (E) Sanger sequencing of the *TIMP3* gene for one hiPSC clone for each patient as well as for Control 1 (RD08A). Substitution of adenine to thymine missense mutation leading to serine to cysteine amino acid substitution in the SFD-hiPSC lines shown. (F) RT-qPCR test for expression of viral vectors in the hiPSC lines after a minimum of 7 passages. Average ct-values for each of the reprogramming vectors shown. Ct-values >35 interpreted as undetected (u.d.). Error bars indicte SD. Human iPSC colonies picked after reprogramming served as a positive PCR control and dH_20 as negative PCR control. Positive expression of *GAPDH* reference gene is shown for all the samples.

Figure S2. Characterization of the SFD-hiPSC clones RD01A and RD01C. (A) Representative phase contrast images showing typical colony morphology on human foreskin feeder cells. (B) Immunofluorescence images of undifferentiated hiPSC colonies showing expression of the pluripotency markers NANOG, OCT-3/4, SSEA-3, SSEA-4, TRA-1-60, and TRA1-81 as well as corresponding images for nuclei counterstained with DAPI. (C) Pluripotency was confirmed by detection of embryonic germ layer markers after EB differentiation *in vitro,* as well as corresponding nuclear stains. Scale bar 200 µm, valid for all images. (D) Karyogram after Giemsa staining, shown for both cell lines. Red arrows indicating the sites of translocation for RD01A (46,X,t(X;4)(p11;p15)), between the short arms of one X chromosome and one chromosome 4 with breakpoints at bands p11 and p15 respectively. Normal diploid, 46, XX karyogram shown for RD01C.

Figure S3. Characterization of the SFD-hiPSC clones RD03A and RD03B. (A) Representative phase contrast images showing typical colony morphology on human foreskin feeder cells. (B) Immunofluorescence images of undifferentiated hiPSC colonies showing expression of the pluripotency markers NANOG, OCT-3/4, SSEA-3, SSEA-4, TRA-1-60, and TRA1-81 as well as corresponding images for nuclei counterstained with DAPI. (C) Pluripotency was confirmed by detection of embryonic germ layer markers after EB differentiation *in vitro*, as well as corresponding nuclear stains. Scale bar 200 µm, valid for all images. (D) Normal diploid karyogram (46, XX) shown after Giemsa staining for RD03A. Red arrows indicate the sites of translocation for RD03B (46,XX,t(2;4)(p23;p1?2)) between the short arms of one chromosome 2 and one chromosome 4 with breakpoints at bands p23 and p1?2 respectively.

Figure S4. Characterization of the SFD-hiPSC clone RD04B and control-hiPSC clone RD08A (Control 1). (A) Representative phase contrast images showing typical colony morphology on human foreskin feeder cells. (B) Immunofluorescence images of undifferentiated hiPSC colonies showing expression of the pluripotency markers NANOG, OCT-3/4, SSEA-3, SSEA-4, TRA-1-60, and TRA1-81 as well as corresponding images for nuclei counterstained with DAPI. (C) Pluripotency was confirmed by detection of embryonic germ layer markers after EB differentiation *in vitro*, as well as corresponding nuclear stains. Scale bar 200 µm, valid for all images. (D) Normal female karyotype for RD04B analysed with KaryoLite BoBs assay. The results are shown relative to karyotypically normal female (/F, red) and male (/M, blue) genomic DNA used as a reference (equal to 1) for each of the 24 chromosomal probes (covering both p and q arms of all chromosomes). Software threshold for changes is shown as a green line, and deviating results in red. Normal diploid, 46, XX karyogram after Giemsa staining for RD08A.

Figure S5. Characterization of the Control-hiPSC lines UTA.04311.WTs (Control 2) and 10211.EURCCs (Control 3). (A) Representative phase contrast images showing typical colony morphology on human foreskin feeder cells. (B) Immunofluorescence images of undifferentiated hiPSC colonies showing expression of the pluripotency markers NANOG, OCT-3/4, SSEA-3, SSEA-4, TRA-1-60, and TRA1-81 as well as corresponding images for nuclei counterstained with DAPI. (C) Pluripotency was confirmed by detection of embryonic germ layer markers after EB differentiation *in vitro*, as well as corresponding nuclear stains. Scale bar 200 µm, valid for all images. (D) Normal female karyotype shown for both hiPSC lines analysed with KaryoLite BoBs assay. The results are shown relative to karyotypically normal female (/F, red) and male (/M, blue) genomic DNA used as a reference (equal to 1) for each of the 24 chromosomal probes (covering both p and q arms of all chromosomes). Software threshold for changes is shown as a green line and deviating results in red.

Figure S6. RPE characteristics. (A) Confocal z-stack images of IF labelling for RPE markers showing polarized apical localization of Na^+K^+-ATPase pump and the visual cycle protein cellular retinaldehyde binding protein (CRALBP), and microvilli marker ezrin. Y–Z confocal sections and x–y maximum intensity projections (MIP) for primary cilia marker ARL13b. Phalloidin detection was included in confocal sections to show cell borders. The phagocytosis ligand tyrosine-protein kinase Mer (MERTK) showed apical localization. All scale bars, 10 µm. (B) Average concentration of PEDF secreted to apical and basal sides is shown for each cell line, separately and combined, to compare secretion between control and SFD-hiPSC-RPE. n=3 or 4 inserts from one differentiation experiment. Average value of each biological replicate per cell line was used for testing statistical significance (n=3 for control and n=5 for SFD). Slightly more PEDF was secreted to the apical side by SFD-hiPSC-RPE (p=0.0150, Mann–Whitney test) compared to control.

Figure S7. The hiPSC-RPE bearing karyotypic translocations (RD01A and RD03B) showed similar RPE properties as the other SFD-hiPSC-RPE lines. (A) DIC images showing RPE morphology and pigmentation pattern (scale bar, 20 µm) and confocal images for RPE marker expression and localization (scale bars, 10 µm for all images). (B) Phagocytic capacity shown after feeding with porcine POS for 4 h, followed by IF labelling with anti-opsin and confocal imaging. White arrows show internalized POS (green). Phalloidin (red) shows cells. Scale bar 10 µm.

Figure S8. TIMP3 expression and secretion. (A) TIMP3 western blotting analysis repeated with another set of samples from a separate differentiation experiment (compare to Figure 4B) using Abcam 39184 antibody. A representative image after long exposure time to visualize the difference in abundance for the 27 kDa glycosylated band. The band intensities were quantified using densitometry, relative to β-actin from non-saturated images for the 27 kDa and 48 kDa bands. No statistically significant difference was reached between SFD and control for glycosylated ($p=0.0714$, Mann–Whitney test) or dimer ($p=1.000$) forms of TIMP3. Monomer was not quantified due to rapid saturation of the strong bands for SFD-hiPSC-RPE samples. (B,C) TIMP3 detection with Abcam ab58804 antibody from two sets of samples from separate differentiation experiments. Extensively exposed blot in (C) to visualise the glycosylated band. A statistically significant difference in expression of the monomer was found between SFD and control ($p=0.0357$ for B and C). (D) TIMP3 secretion measured by ELISA from hiPSC-RPE cultured on permeable cell culture inserts. + denotes the mean value. Median values are shown above the plot for both SFD-hiPSC-RPE and control-hiPSC-RPE **$p=0.0079$. Error bars show SD. n=number of inserts (number of cell lines).

Figure S9. EnzCheck collagenase assay results shown for each cell line individually. Collagenase/gelatinase (MMP) activity against quenched fluorescein-conjugated DQ gelatin was measured as fluorescence intensity. Addition of the general MMP inhibitor 1,10-phenanthroline (+inhibitor) or conditioned media (CM) from hiPSC-RPE containing 50 ng TIMP3, showed a decrease in fluorescence relative to no inhibitor, indicating MMP inhibition. All control clones exhibited higher gelatinase activity than all SFD clones. Error bars show SD.

Figure S10. Proteomic profiling of SFD-hiPSC-RPE comparing to control-hiPSC-RPE. (A) Pie chart showing the proportions of the proteins upregulated (red) and downregulated (green) according to fold-change difference ≥1.5, by SFD compared control. (B) DAVID functional annotation clustering of the 89 differentially expressed proteins (red and green) in SFD and control showed three enriched clusters relating to ECM, cytoskeleton, and cell adhesion and junctions. (C) Fibulin-3 was 1.3-fold upregulated according to proteomics and (D) upregulation was confirmed by western blotting. (E) Quantification by densitometry showing relative expression normalized to β-actin loading control. Error bars show SD. (F) Apolipoprotein E (APOE) was 1.7-fold upregulated in our proteomics study and (G,H) showed slight upregulation also by western blotting.

Figure S11. TIMP3 was initially filtered out of the analysed data during stringent CV filtering. (A) A scatter plot showing proteomics quantitation results for TIMP3 on a log2 scale with TIMP3 showing 1.7-fold increase in expression compared to control, and (B) representative chromatography peaks for TIMP3 for each cell line are shown.

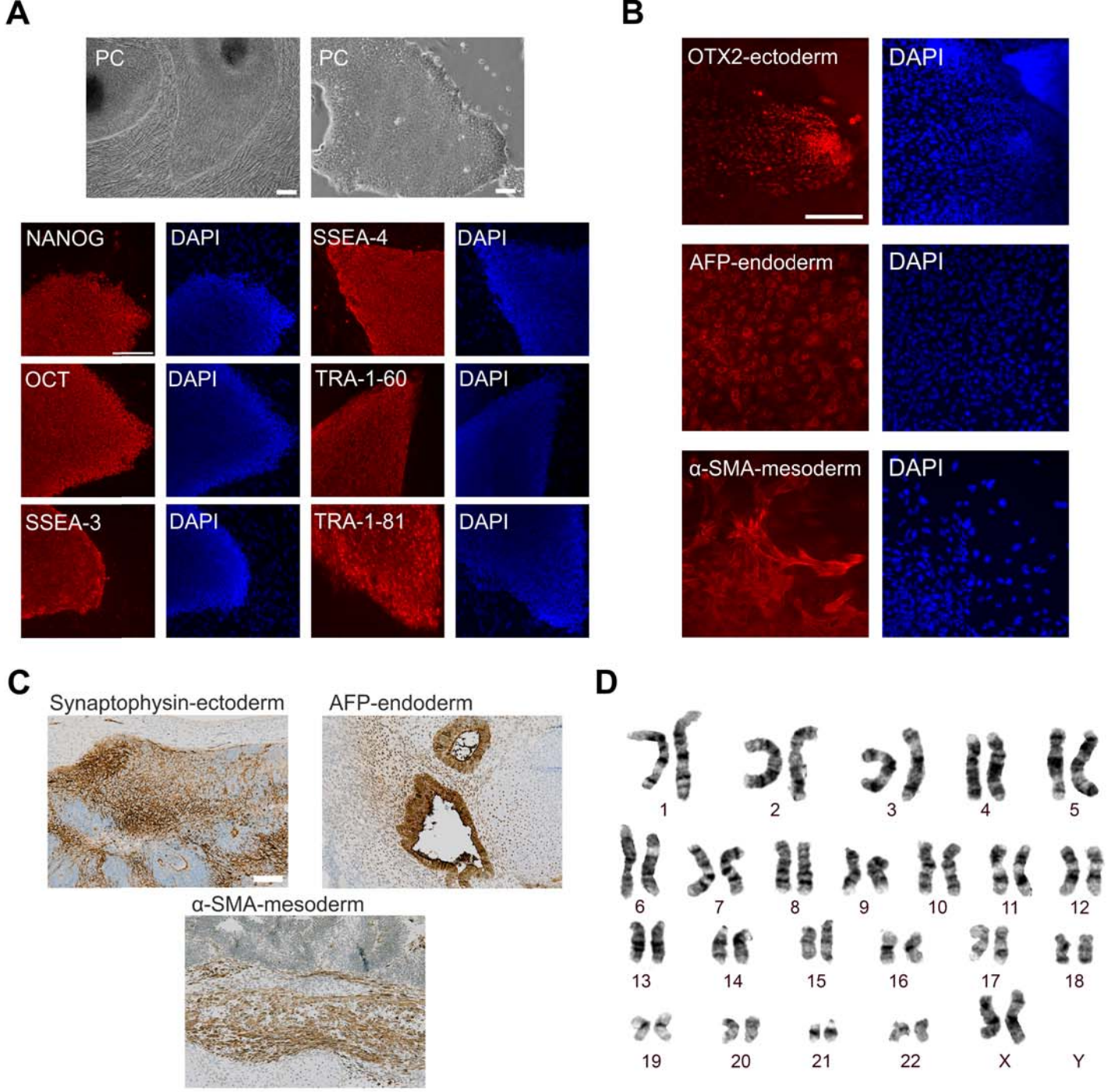
A
PC
PC
NANOG
DAPI
SSEA-4
DAPI
OCT
DAPI
TRA-1-60
DAPI
SSEA-3
DAPI
TRA-1-81
DAPI
B
OTX2-ectoderm
DAPI
AFP-endoderm
DAPI
α-SMA-mesoderm
DAPI
C
Synaptophysin-ectoderm
AFP-endoderm
α-SMA-mesoderm
D
1
2
3
4
5
6
7
8
9
10
11
12
13
14
15
16
17
18
19
20
21
22
X
Y
E
A/T
110
120
130
C C C G G A T A A A M G C A T C A T C A A
RD04A
C C C G G A T A A A T G C A T C A T C A A
Control 1
C C C G G A T A A A A G C A T C A T C A A
RD01C
C C C G G A T A A A N G C A T C A T C A A
RD03A
C C C G G A T A A A T G C A T C A T C A A
F
GAPDH
SEV
C-MYC
KLF-4
KOS
Ct-value
35
30
25
20
15
10
5
0
u.d.
Pos. PCR control
Control 1
Control 2
Control 3
RD04A
RD04B
RD03A
RD03B
RD01A
RD01C
H2O

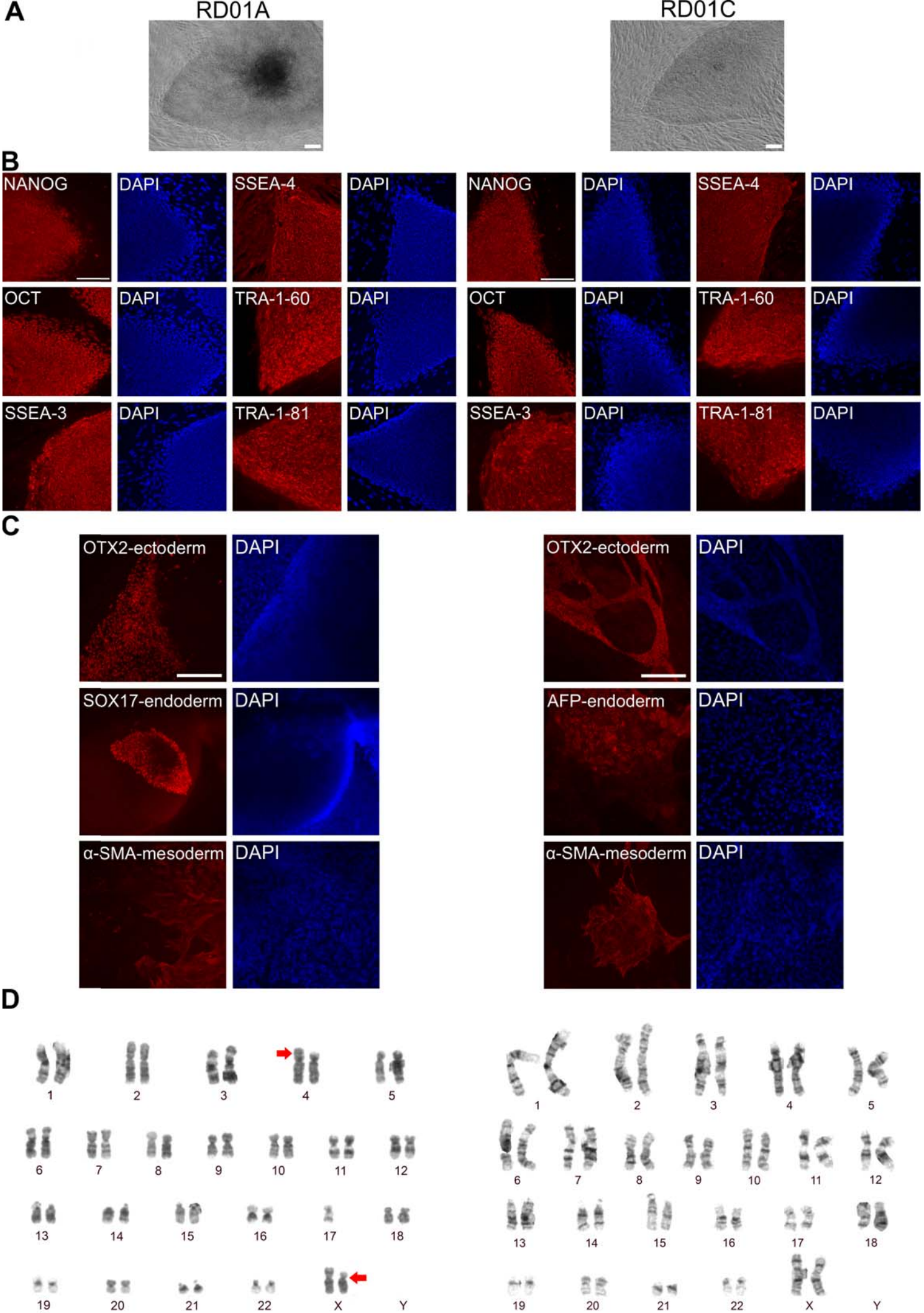
A
RD01A
RD01C
B
NANOG
DAPI
SSEA-4
DAPI
NANOG
DAPI
SSEA-4
DAPI
OCT
DAPI
TRA-1-60
DAPI
OCT
DAPI
TRA-1-60
DAPI
SSEA-3
DAPI
TRA-1-81
DAPI
SSEA-3
DAPI
TRA-1-81
DAPI
C
OTX2-ectoderm
DAPI
OTX2-ectoderm
DAPI
SOX17-endoderm
DAPI
AFP-endoderm
DAPI
α-SMA-mesoderm
DAPI
α-SMA-mesoderm
DAPI
D
1
2
3
4
5
6
7
8
9
10
11
12
13
14
15
16
17
18
19
20
21
22
X
Y
1
2
3
4
5
6
7
8
9
10
11
12
13
14
15
16
17
18
19
20
21
22
X
Y

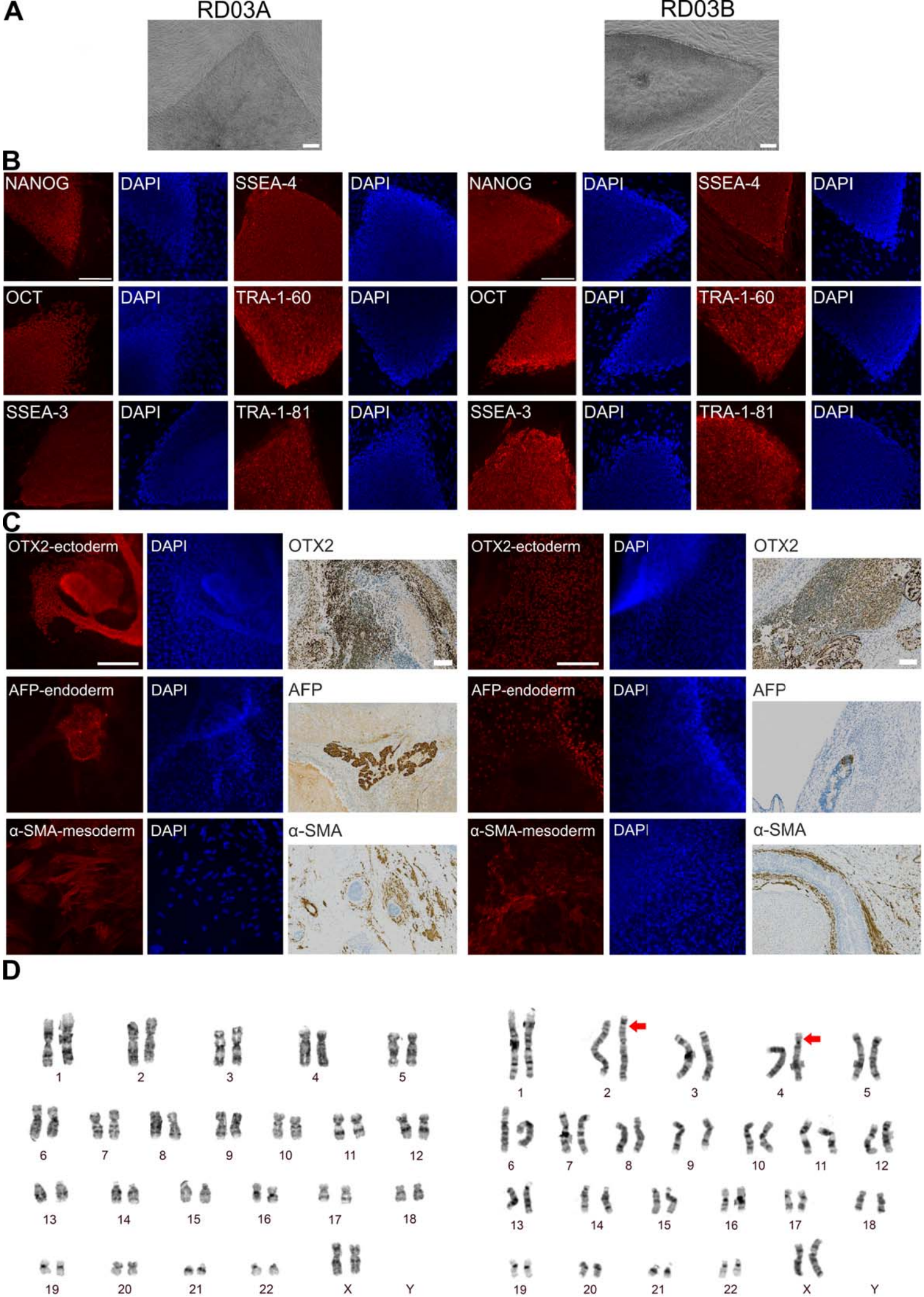
A
RD03A
RD03B
B
NANOG
DAPI
SSEA-4
DAPI
NANOG
DAPI
SSEA-4
DAPI
OCT
DAPI
TRA-1-60
DAPI
OCT
DAPI
TRA-1-60
DAPI
SSEA-3
DAPI
TRA-1-81
DAPI
SSEA-3
DAPI
TRA-1-81
DAPI
C
OTX2-ectoderm
DAPI
OTX2
OTX2-ectoderm
DAPI
OTX2
AFP-endoderm
DAPI
AFP
AFP-endoderm
DAPI
AFP
α-SMA-mesoderm
DAPI
α-SMA
α-SMA-mesoderm
DAPI
α-SMA
D
1
2
3
4
5
6
7
8
9
10
11
12
13
14
15
16
17
18
19
20
21
22
X
Y
1
2
3
4
5
6
7
8
9
10
11
12
13
14
15
16
17
18
19
20
21
22
X
Y

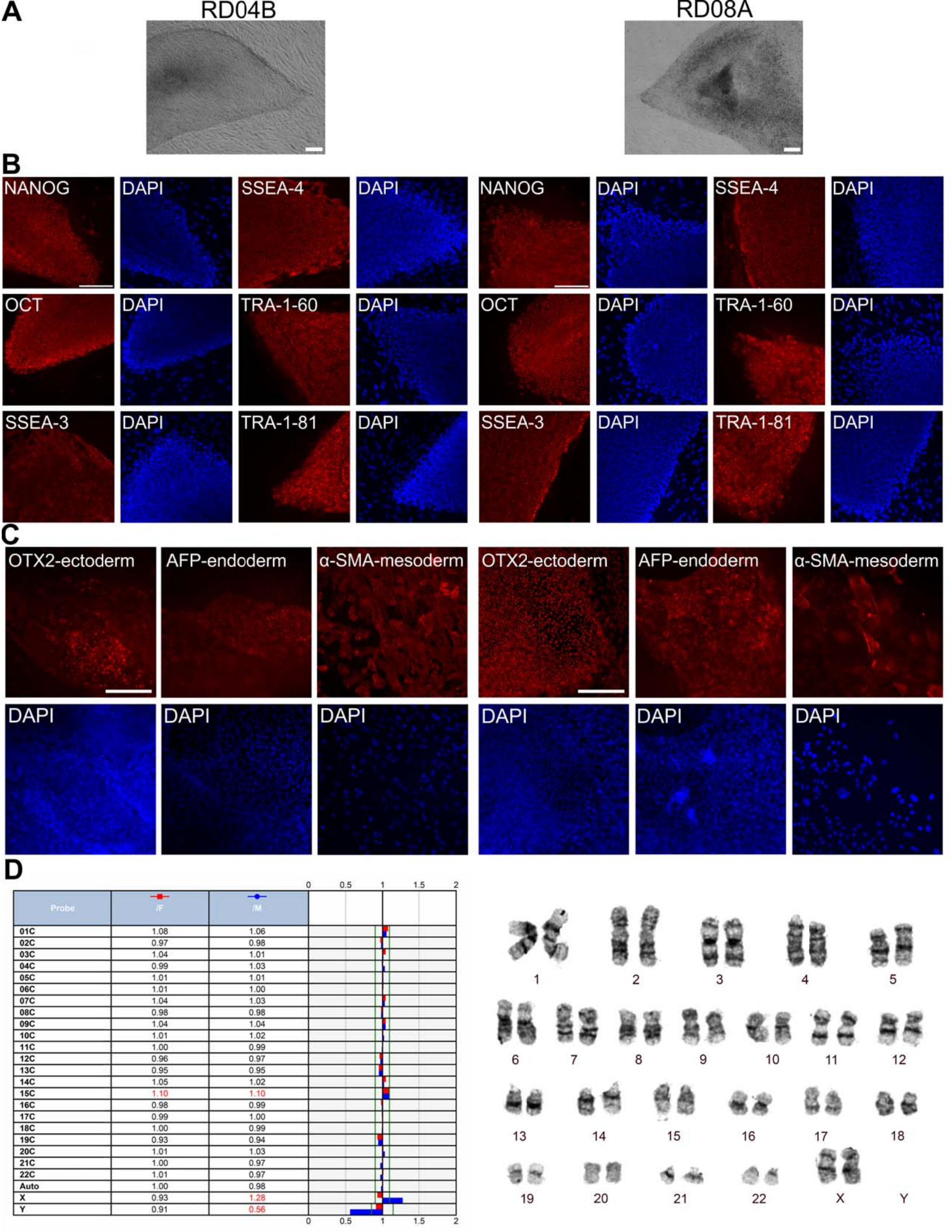

Probe	/F	/M
01C	1.08	1.06
02C	0.97	0.98
03C	1.04	1.01
04C	0.99	1.03
05C	1.01	1.01
06C	1.01	1.00
07C	1.04	1.03
08C	0.98	0.98
09C	1.04	1.04
10C	1.01	1.02
11C	1.00	0.99
12C	0.96	0.97
13C	0.95	0.95
14C	1.05	1.02
15C	1.10	1.10
16C	0.98	0.99
17C	0.99	1.00
18C	1.00	0.99
19C	0.93	0.94
20C	1.01	1.03
21C	1.00	0.97
22C	1.01	0.97
Auto	1.00	0.98
X	0.93	1.28
Y	0.91	0.56

A

B

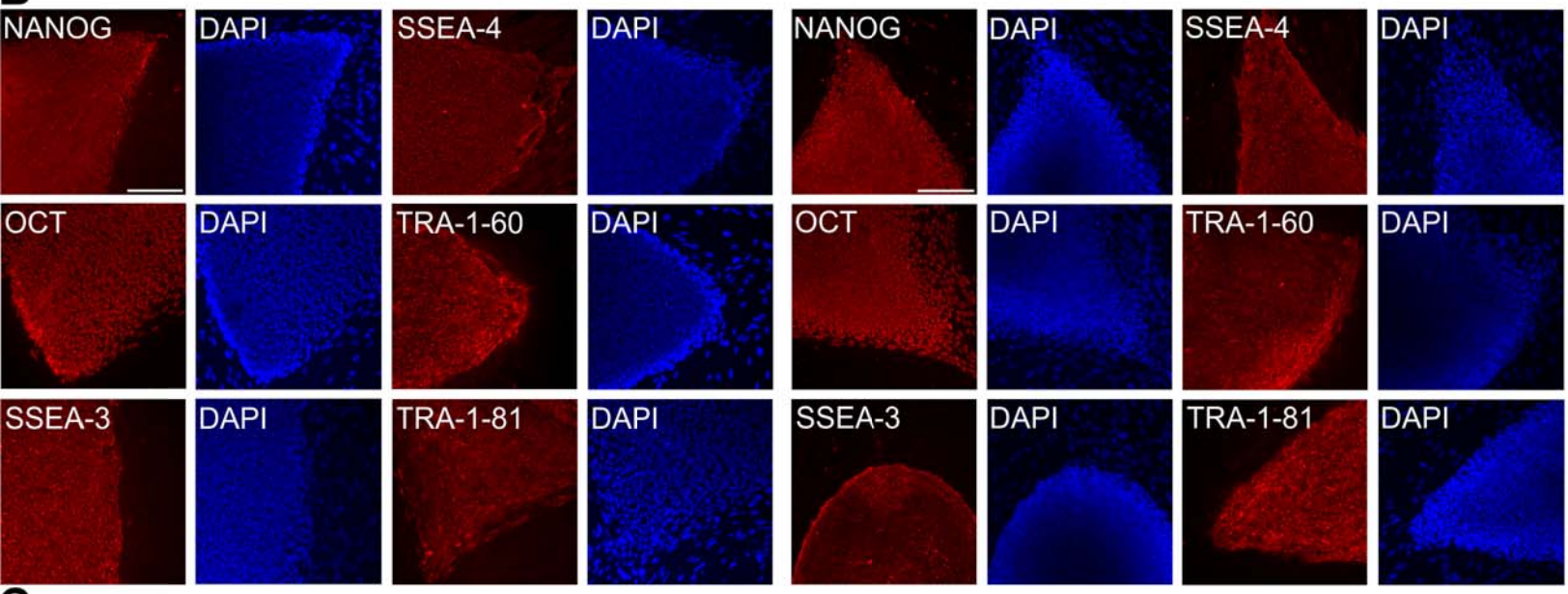

C

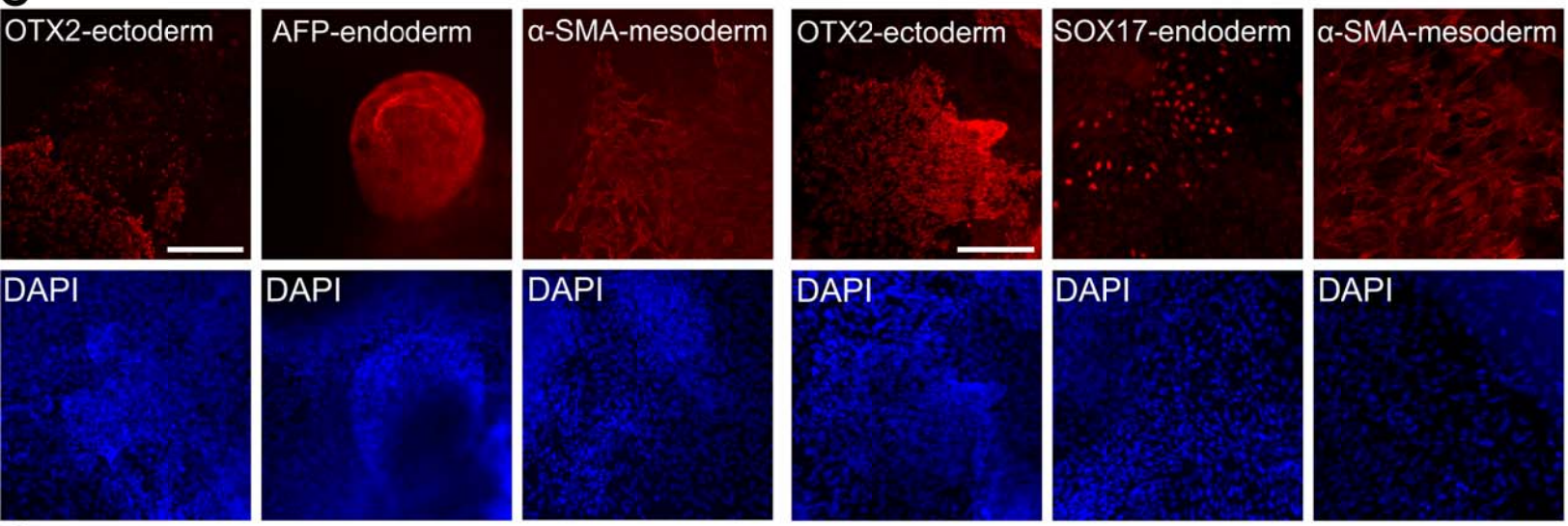

D

Probe	/F	/M
01C	1.00	1.02
02C	1.04	1.03
03C	1.07	1.04
04C	1.07	1.07
05C	0.99	1.02
06C	1.02	1.05
07C	0.96	0.99
08C	0.95	0.95
09C	1.03	1.05
10C	1.04	1.01
11C	1.02	1.02
12C	1.03	1.02
13C	0.95	1.01
14C	1.06	1.05
15C	1.07	1.07
16C	1.05	1.04
17C	1.02	1.03
18C	0.97	1.00
19C	1.04	1.02
20C	1.09	1.05
21C	0.98	1.00
22C	1.04	1.05
Auto	0.95	0.95
X	1.01	1.56
Y	1.06	0.48

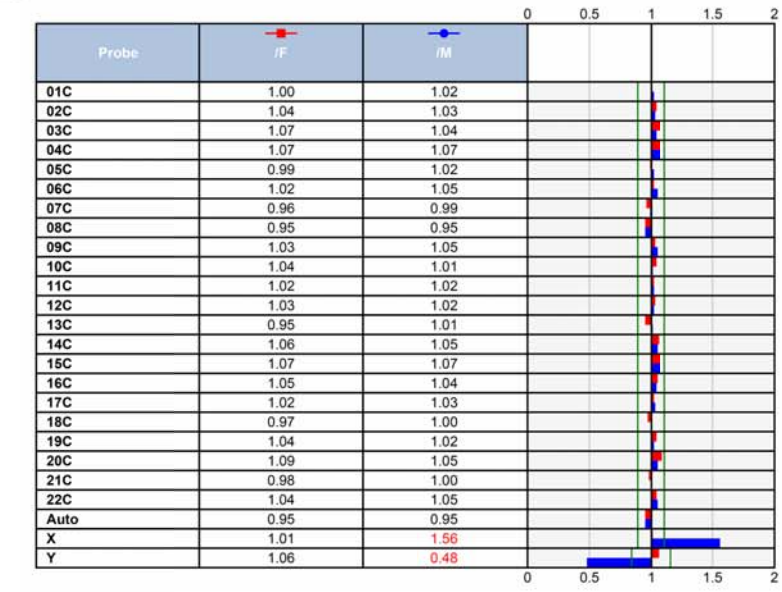

Probe	/F	/M
01C	1.01	1.02
02C	1.00	1.03
03C	1.00	1.00
04C	0.97	0.95
05C	0.98	1.01
06C	0.99	1.01
07C	1.00	0.99
08C	0.94	0.98
09C	1.05	1.03
10C	0.98	0.98
11C	0.95	0.99
12C	0.97	0.98
13C	0.97	0.99
14C	1.03	1.02
15C	1.04	1.05
16C	0.99	1.03
17C	1.00	1.01
18C	0.98	0.99
19C	0.98	1.03
20C	1.03	1.04
21C	1.04	1.03
22C	1.03	1.04
Auto	0.97	0.98
X	0.92	1.45
Y	1.16	0.46

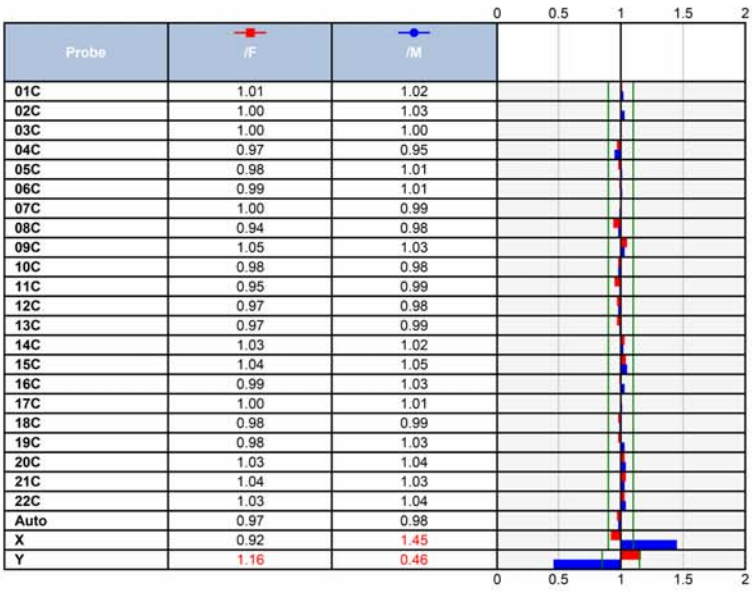

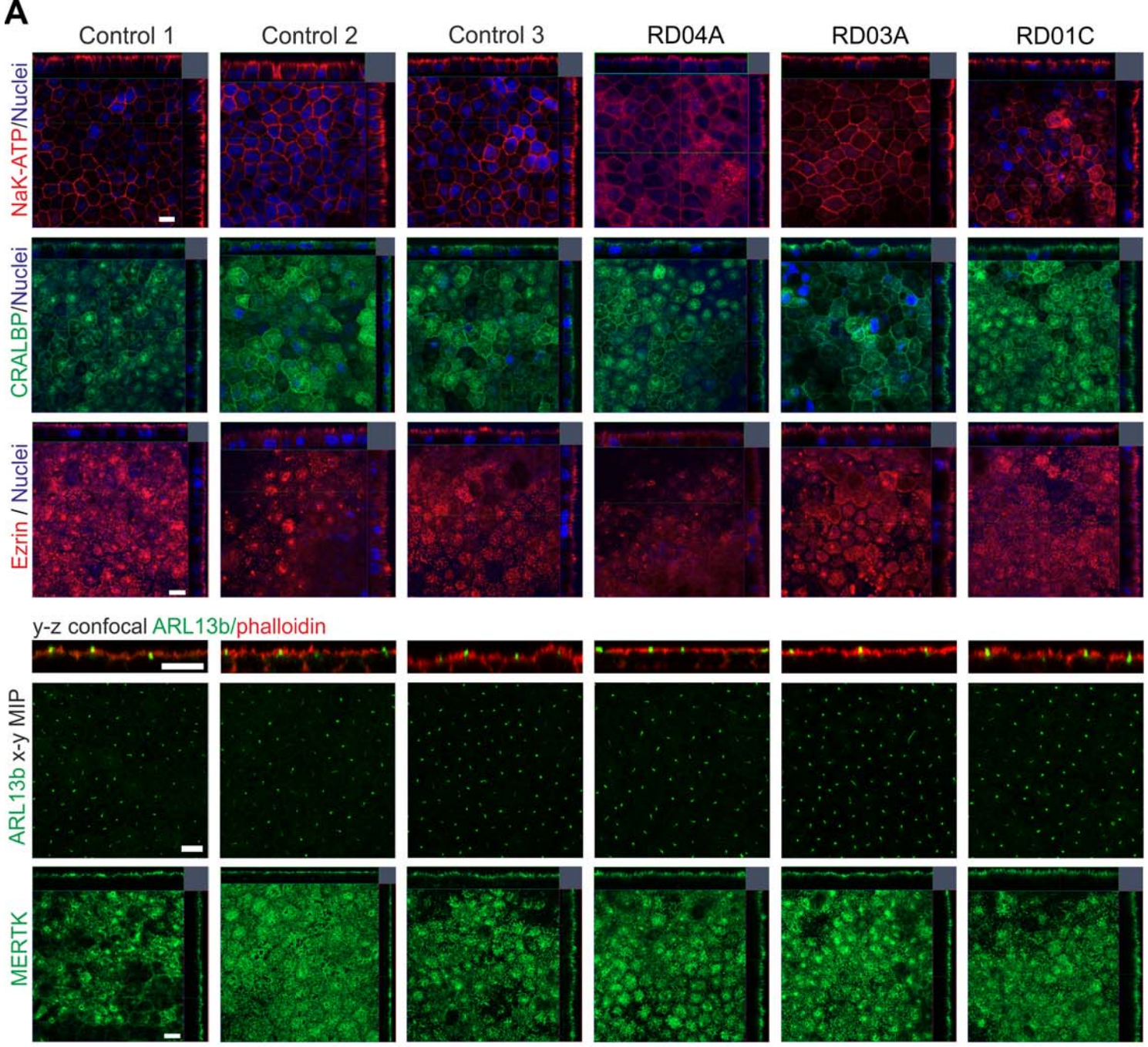
A
Control 1
Control 2
Control 3
RD04A
RD03A
RD01C
NaK-ATP/Nuclei
CRALBP/Nuclei
Ezrin / Nuclei
y-z confocal ARL13b/phalloidin
ARL13b x-y MIP
MERTK

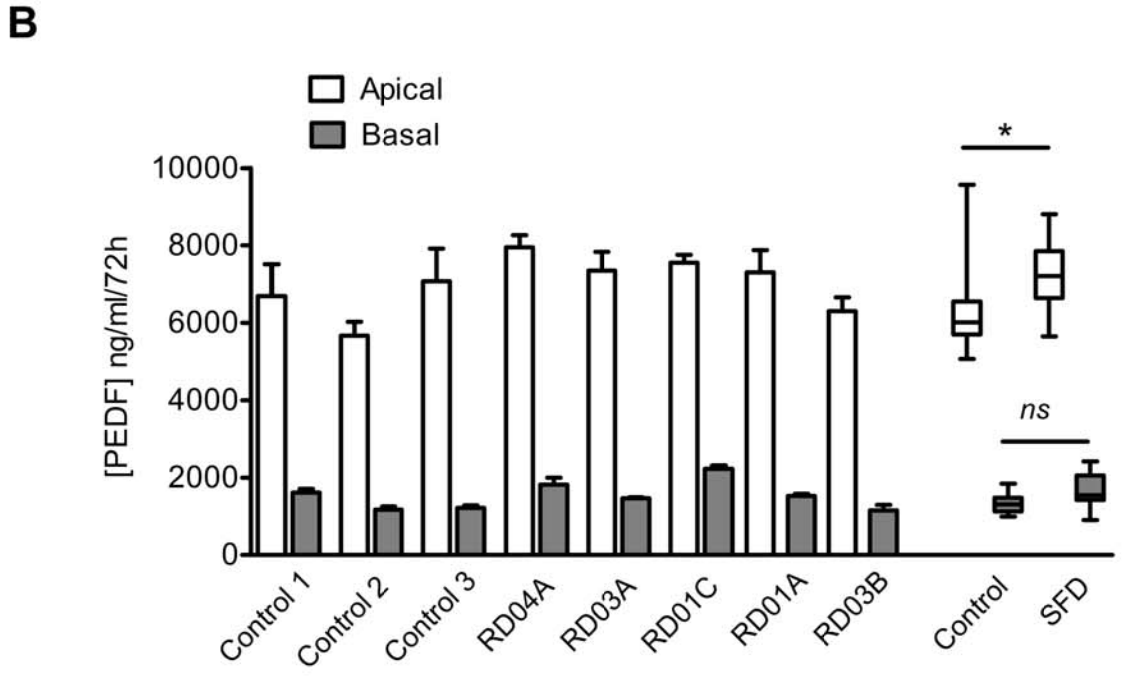
B
Apical
Basal
[PEDF] ng/ml/72h
10000
8000
6000
4000
2000
0
*
ns
Control 1
Control 2
Control 3
RD04A
RD03A
RD01C
RD01A
RD03B
Control
SFD

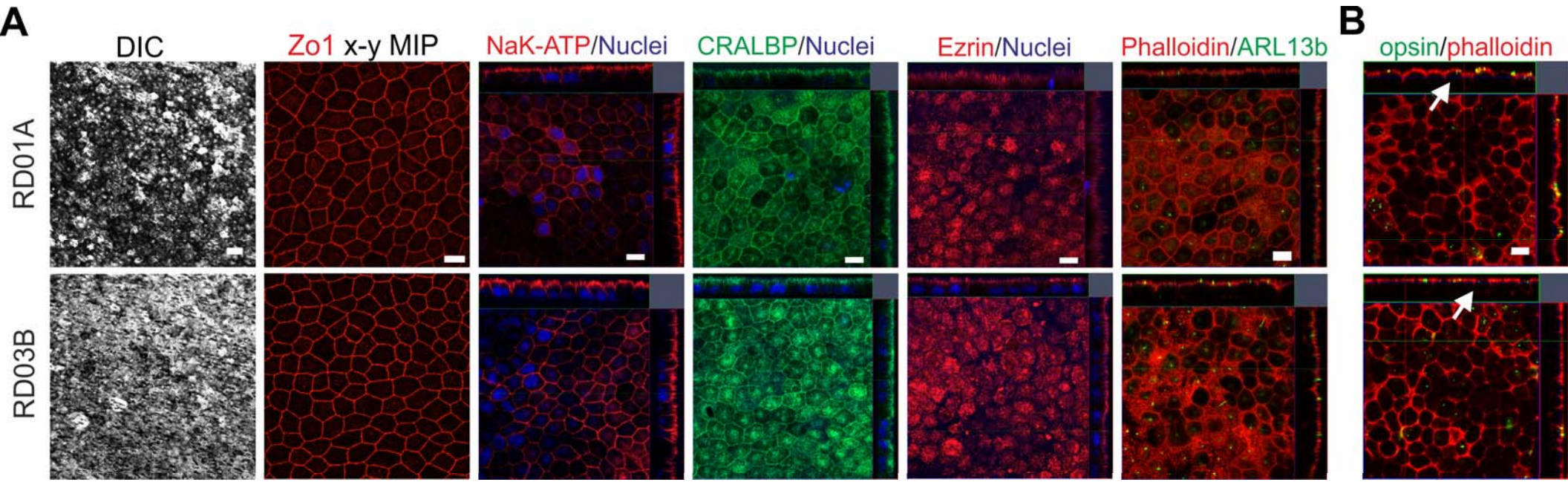
A
DIC
Zo1 x-y MIP
NaK-ATP/Nuclei
CRALBP/Nuclei
Ezrin/Nuclei
Phalloidin/ARL13b
B
opsin/phalloidin
RD01A
RD03B

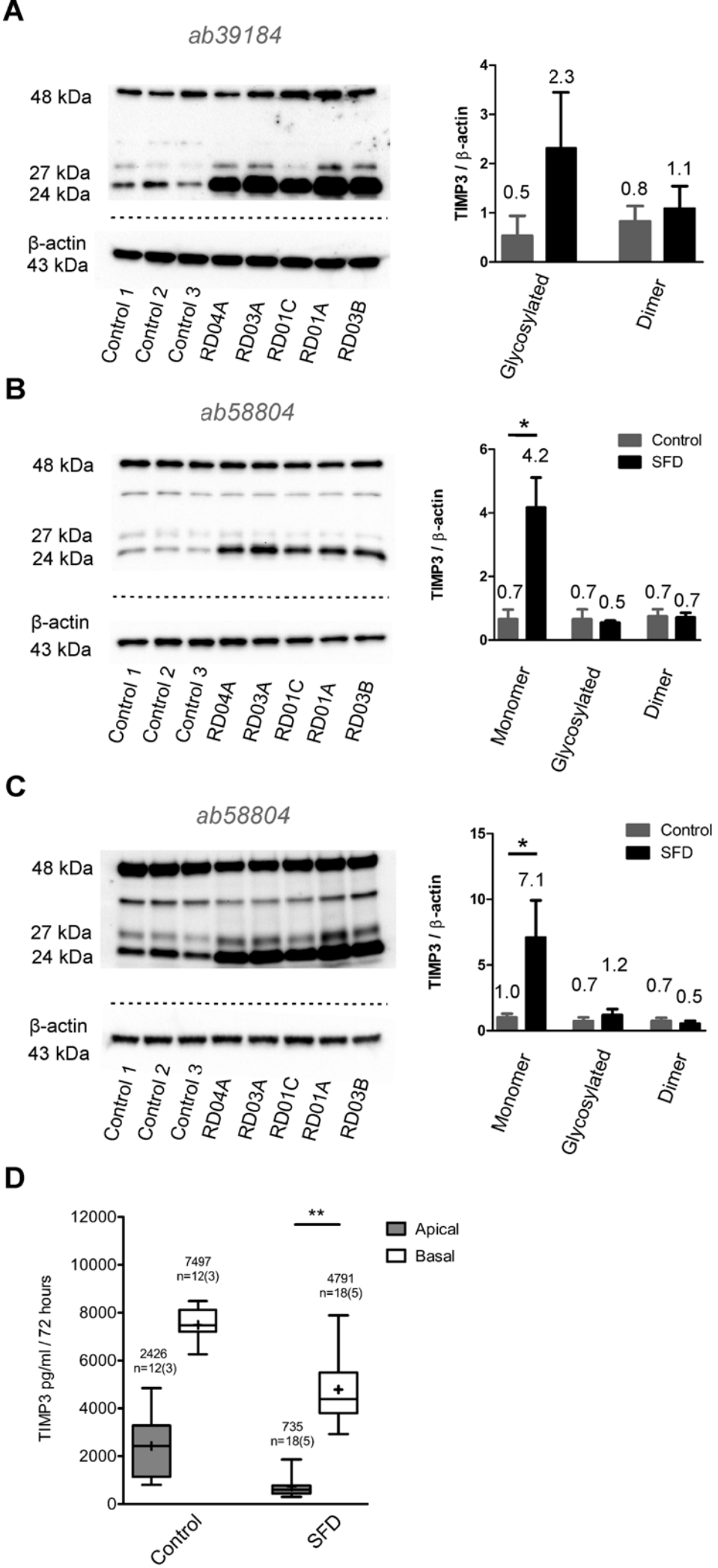
A
ab39184
48 kDa
27 kDa
24 kDa
β-actin
43 kDa
Control 1
Control 2
Control 3
RD04A
RD03A
RD01C
RD01A
RD03B
TIMP3 / β-actin
0.5
2.3
0.8
1.1
Glycosylated
Dimer
B
ab58804
48 kDa
27 kDa
24 kDa
β-actin
43 kDa
Control 1
Control 2
Control 3
RD04A
RD03A
RD01C
RD01A
RD03B
*
Control
SFD
TIMP3 / β-actin
0.7
4.2
0.7
0.5
0.7
0.7
Monomer
Glycosylated
Dimer
C
ab58804
48 kDa
27 kDa
24 kDa
β-actin
43 kDa
Control 1
Control 2
Control 3
RD04A
RD03A
RD01C
RD01A
RD03B
*
Control
SFD
TIMP3 / β-actin
1.0
7.1
0.7
1.2
0.7
0.5
Monomer
Glycosylated
Dimer
D
**
Apical
Basal
TIMP3 pg/ml / 72 hours
7497
n=12(3)
2426
n=12(3)
4791
n=18(5)
735
n=18(5)
Control
SFD

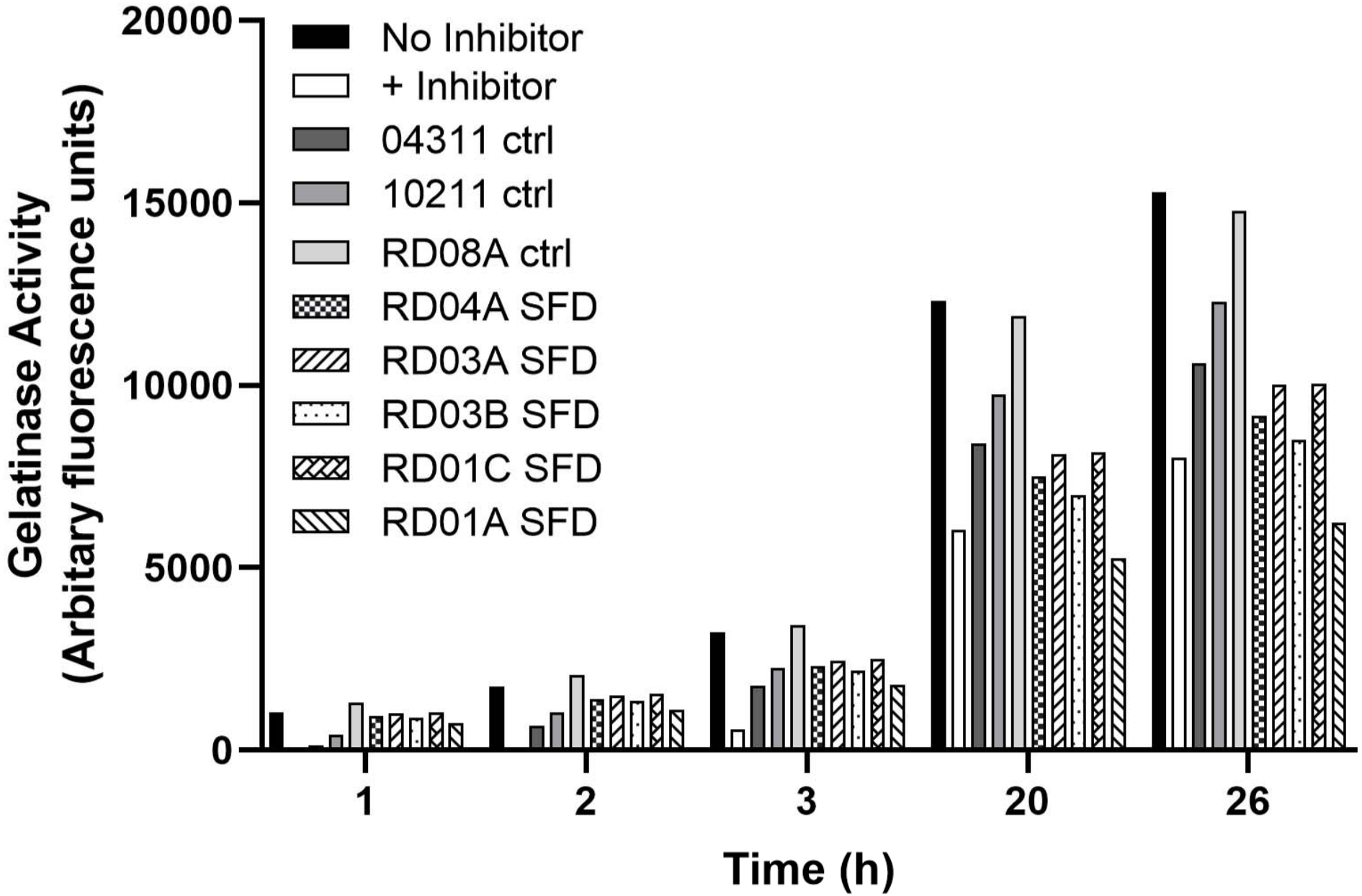
Gelatinase Activity
(Arbitary fluorescence units)
20000
15000
10000
5000
0
No Inhibitor
+ Inhibitor
04311 ctrl
10211 ctrl
RD08A ctrl
RD04A SFD
RD03A SFD
RD03B SFD
RD01C SFD
RD01A SFD
1
2
3
20
26
Time (h)

A

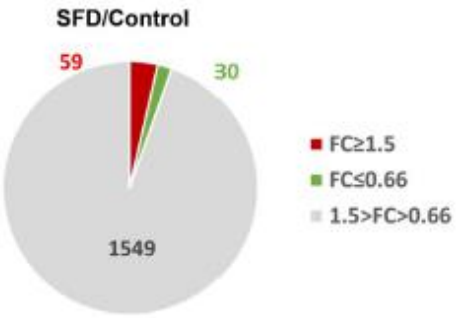

B

Annotation Cluster 1	Enrichment Score: 4.84	G		Count	P_Value	Benjamini
GOTERM_CC_DIRECT	extracellular matrix	RT		12	1.4E-7	1.3E-5
GOTERM_CC_DIRECT	extracellular space	RT		19	4.7E-5	1.7E-3
GOTERM_CC_DIRECT	extracellular region	RT		19	4.4E-4	1.3E-2
Annotation Cluster 2	Enrichment Score: 2.72	G		Count	P_Value	Benjamini
GOTERM_CC_DIRECT	stress fiber	RT		6	5.5E-6	2.5E-4
GOTERM_MF_DIRECT	actin binding	RT		6	1.3E-2	6.5E-1
GOTERM_CC_DIRECT	cytoskeleton	RT		5	9.8E-2	5.5E-1
Annotation Cluster 3	Enrichment Score: 1.56	G		Count	P_Value	Benjamini
GOTERM_BP_DIRECT	cell-cell adhesion	RT		6	1.2E-2	8.4E-1
GOTERM_MF_DIRECT	cadherin binding involved in cell-cell adhesion	RT		6	1.6E-2	5.2E-1
GOTERM_CC_DIRECT	cell-cell adherens junction	RT		6	1.8E-2	2.5E-1
GOTERM_CC_DIRECT	cell-cell junction	RT		4	4.8E-2	3.8E-1
GOTERM_CC_DIRECT	cytoskeleton	RT		5	9.8E-2	5.5E-1

C

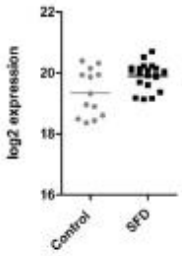

D

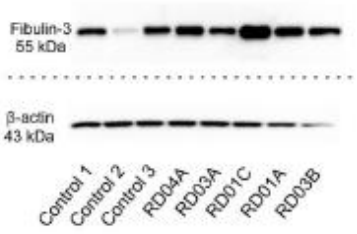

E

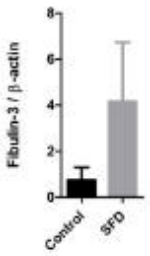

F

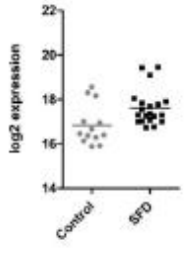

G

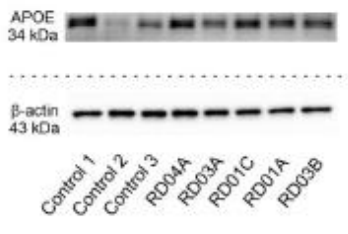

H

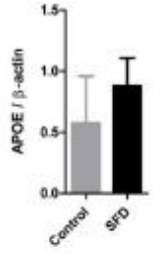

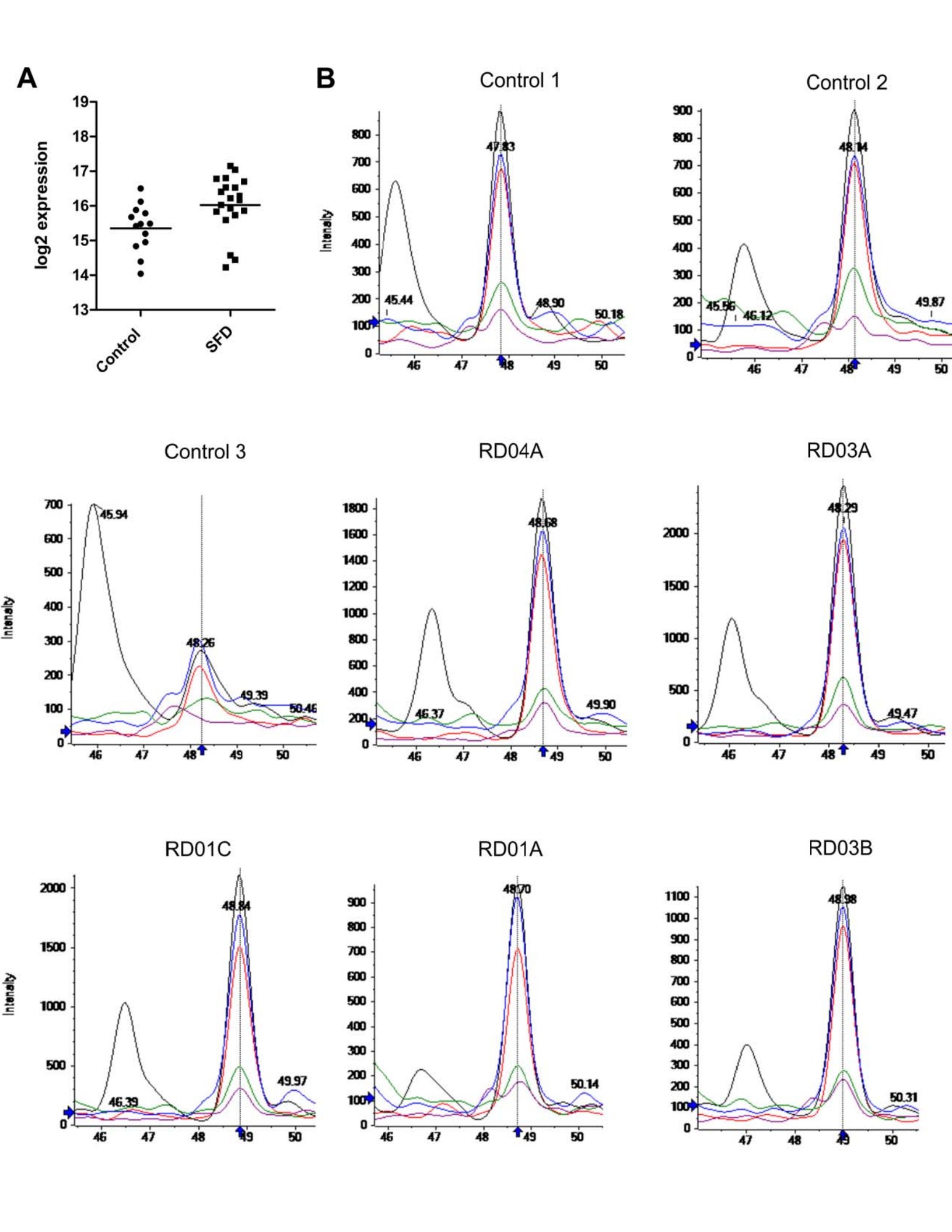
A
log2 expression
19
18
17
16
15
14
13
Control
SFD
B
Control 1
Control 2
Control 3
RD04A
RD03A
RD01C
RD01A
RD03B
Intensity
45.44
47.83
48.90
50.18
45.56
46.12
48.14
49.87
45.94
48.26
49.39
50.46
46.37
48.68
49.90
48.29
49.47
46.39
48.84
49.97
48.70
50.14
48.98
50.31

Supplementary Table 1. Differentially expressed proteins according to fold change in SFD-hiPSC-RPE/Control-hiPSC-RPE.
Proteins upregulated = fold change (FC) ≥1.5 (red background) and downregulated FC ≤0.66 (green background)

Uniprot	Description	Symbol	Fold change (disease/control)
Q08431	Lactadherin	MFGE8	4.75
P02452	Collagen alpha-1(I) chain	COL1A1	4.00
Q01995	Transgelin	TAGLN	3.05
Q8IUX7	Adipocyte enhancer-binding protein 1	AEBP1	2.82
P54652	Heat shock-related 70 kDa protein 2	HSPA2	2.58
Q04695	Keratin, type I cytoskeletal 17	KRT17	2.41
Q15746	Myosin light chain kinase, smooth muscle	MYLK	2.33
P09493	Tropomyosin alpha-1 chain	TPM1	2.22
P35749	Myosin-11	MYH11	2.19
Q9UK22	F-box only protein 2	FBXO2	2.16
Q99715	Collagen alpha-1(XII) chain	COL12A1	2.12
Q5EB52	Mesoderm-specific transcript homolog protein	MEST	2.05
Q92765	Secreted frizzled-related protein 3	FRZB	2.04
Q92626	Peroxidasin homolog	PXDN	1.98
Q9NR12	PDZ and LIM domain protein 7	PDLIM7	1.93
Q66K79	Carboxypeptidase Z	CPZ	1.91
Q16527	Cysteine and glycine-rich protein 2	CSRP2	1.89
Q9NZ08	Endoplasmic reticulum aminopeptidase 1	ERAP1	1.85
Q02509	Otoconin-90	OC90	1.85
P54760	Ephrin type-B receptor 4	EPHB4	1.79
P00167	Cytochrome b5	CYB5A	1.76
P36269	Glutathione hydrolase 5 proenzyme	GGT5	1.73
Q14112	Nidogen-2	NID2	1.73
Q15165	Serum paraoxonase/arylesterase 2	PON2	1.72
Q14767	Latent-transforming growth factor beta-binding protein 2	LTBP2	1.71
Q05682	Caldesmon	CALD1	1.70
Q8IWU6	Extracellular sulfatase Sulf-1	SULF1	1.68
P02649	Apolipoprotein E	APOE	1.68
Q16658	Fascin	FSCN1	1.68
Q14BN4	Sarcolemmal membrane-associated protein	SLMAP	1.68
P12271	Retinaldehyde-binding protein 1	RLBP1	1.67
P47804	RPE-retinal G protein-coupled receptor	RGR	1.65
P24593	Insulin-like growth factor-binding protein 5	IGFBP5	1.65
P00450	Ceruloplasmin	CP	1.65
P39060	Collagen alpha-1(XVIII) chain	COL18A1	1.64
Q6UW63	KDEL motif-containing protein 1	KDELC1	1.64
Q96Q06	Perilipin-4	PLIN4	1.62
O75781	Paralemmin-1	PALM	1.61
P11047	Laminin subunit gamma-1	LAMC1	1.61
Q63ZY3	KN motif and ankyrin repeat domain-containing protein 2	KANK2	1.61
P54687	Branched-chain-amino-acid aminotransferase, cytosolic	BCAT1	1.60
Q5TFQ8	Signal-regulatory protein beta-1 isoform 3	SIRPB1	1.60
Q13642	Four and a half LIM domains protein 1	FHL1	1.60
P21291	Cysteine and glycine-rich protein 1	CSRP1	1.59
P50479	PDZ and LIM domain protein 4	PDLIM4	1.58
P63218	Guanine nucleotide-binding protein G(I)/G(S)/G(O) subunit gamma-5	GNG5	1.58
Q9HAV0	Guanine nucleotide-binding protein subunit beta-4	GNB4	1.57
Q16270	Insulin-like growth factor-binding protein 7	IGFBP7	1.57
P50225	Sulfotransferase 1A1	SULT1A1	1.56
P09669	Cytochrome c oxidase subunit 6C	COX6C	1.56
Q14289	Protein-tyrosine kinase 2-beta	PTK2B	1.56
Q05707	Collagen alpha-1(XIV) chain	COL14A1	1.55
Q99439	Calponin-2	CNN2	1.54
P55196	Afadin	AFDN	1.53
Q12860	Contactin-1	CNTN1	1.52
P24844	Myosin regulatory light polypeptide 9	MYL9	1.52
Q9P2B2	Prostaglandin F2 receptor negative regulator	PTGFRN	1.52
Q92643	GPI-anchor transamidase	PIGK	1.51
Q96FV2	Secernin-2	SCRN2	1.50
Q9NVS2	39S ribosomal protein S18a, mitochondrial	MRPS18A	0.66
Q9Y305	Acyl-coenzyme A thioesterase 9, mitochondrial	ACOT9	0.66
O14975	Very long-chain acyl-CoA synthetase	SLC27A2	0.66
P15289	Arylsulfatase A	ARSA	0.66
Q99541	Perilipin-2	PLIN2	0.66
Q86V81	THO complex subunit 4	ALYREF	0.66
P16219	Short-chain specific acyl-CoA dehydrogenase, mitochondrial	ACADS	0.65
P29972	Aquaporin-1	AQP1	0.64
P11908	Ribose-phosphate pyrophosphokinase 2	PRPS2	0.64
Q92781	11-cis retinol dehydrogenase	RDH5	0.64
Q96BI1	Solute carrier family 22 member 18	SLC22A18	0.63
O95831	Apoptosis-inducing factor 1, mitochondrial	AIFM1	0.62
P53634	Dipeptidyl peptidase 1	CTSC	0.62
Q2TB90	Putative hexokinase HKDC1	HKDC1	0.61
Q93008	Probable ubiquitin carboxyl-terminal hydrolase FAF-X	USP9X	0.60
Q92597	Protein NDRG1	NDRG1	0.60
Q01844	RNA-binding protein EWS	EWSR1	0.60
Q05469	Hormone-sensitive lipase	LIPE	0.59
Q9BTZ2	Dehydrogenase/reductase SDR family member 4	DHRS4	0.59
Q9HA77	Probable cysteine--tRNA ligase, mitochondrial	CARS2	0.58
P54868	Hydroxymethylglutaryl-CoA synthase, mitochondrial	HMGCS2	0.57
P35637	RNA-binding protein FUS	FUS	0.57
Q12955	Ankyrin-3	ANK3	0.56
P01892	HLA class I histocompatibility antigen, A-2 alpha chain	HLA-A	0.53
Q92522	Histone H1x	H1FX	0.53
P09038	Fibroblast growth factor 2	FGF2	0.52
P17096	High mobility group protein HMG-I/HMG-Y	HMGA1	0.51
P30459	HLA class I histocompatibility antigen, A-74 alpha chain	HLA-A	0.50
P27338	Amine oxidase [flavin-containing] B	MAOB	0.48
Q8TB22	Spermatogenesis-associated protein 20	SPATA20	0.48

Supplementary Table 2. Differentially expressed proteins according to statistical significance (LMER linear mixed effects model) in SFD-hiPSC-RPE/Control-hiPSC-RPE.
Proteins with model coefficient fold change values with p-value <0.01 (darker blue background) and p<0.05 (lighter blue background).

			Model Coefficient	
Uniprot	**Full name**	**Symbol**	**Fold Change SFD/Control**	**P-value**
P16144	Integrin beta-4	ITGB4	1.46	0.000
Q8IWU6	Extracellular sulfatase Sulf-1	SULF1	1.65	0.000
O00571	ATP-dependent RNA helicase DDX3X	DDX3X	0.82	0.000
Q8NFZ8	Cell adhesion molecule 4	CADM4	1.24	0.000
P48449	Lanosterol synthase	LSS	1.24	0.000
Q9NZ08	Endoplasmic reticulum aminopeptidase 1	ERAP1	2.33	0.000
Q9BTU6	Phosphatidylinositol 4-kinase type 2-alpha	PI4K2A	0.71	0.000
P50479	PDZ and LIM domain protein 4	PDLIM4	1.52	0.001
Q13425	Beta-2-syntrophin	SNTB2	1.15	0.001
Q8TCT9	Minor histocompatibility antigen H13	HM13	0.75	0.001
Q13418	Integrin-linked protein kinase	ILK	1.46	0.001
Q02878	60S ribosomal protein L6	RPL6	1.16	0.002
P54687	Branched-chain-amino-acid aminotransferase, cytosolic	BCAT1	1.57	0.002
P08134	Rho-related GTP-binding protein RhoC	RHOC	1.28	0.002
Q53GS9	U4/U6.U5 tri-snRNP-associated protein 2	USP39	0.73	0.002
Q99541	Perilipin-2	PLIN2	0.68	0.002
P09543	2',3'-cyclic-nucleotide 3'-phosphodiesterase	CNP	1.18	0.002
P10606	Cytochrome c oxidase subunit 5B, mitochondrial	COX5B	1.50	0.002
P04181	Ornithine aminotransferase, mitochondrial	OAT	0.84	0.002
Q02809	Procollagen-lysine,2-oxoglutarate 5-dioxygenase 1	PLOD1	1.38	0.002
P62241	40S ribosomal protein S8	RPS8	0.80	0.002
Q96FV2	Secernin-2	SCRN2	1.54	0.002
Q9UK22	F-box only protein 2	FBXO2	2.04	0.003
Q9Y394	Dehydrogenase/reductase SDR family member 7	DHRS7	0.75	0.003
P28838	Cytosol aminopeptidase	LAP3	0.84	0.003
Q02318	Sterol 26-hydroxylase, mitochondrial	CYP27A1	0.82	0.003
Q9P0I2	ER membrane protein complex subunit 3	EMC3	0.76	0.003
P10620	Microsomal glutathione S-transferase 1	MGST1	0.71	0.003
Q5VWZ2	Lysophospholipase-like protein 1	LYPLAL1	0.69	0.004
P00450	Ceruloplasmin	CP	1.67	0.004
Q96A33	Coiled-coil domain-containing protein 47	CCDC47	0.84	0.004
P36269	Glutathione hydrolase 5 proenzyme	GGT5	1.67	0.005
P16402	Histone H1.3	HIST1H1D	0.69	0.006
P38919	Eukaryotic initiation factor 4A-III	EIF4A3	1.19	0.006
Q6UW63	KDEL motif-containing protein 1	KDELC1	1.62	0.007
Q92598	Heat shock protein 105 kDa	HSPH1	0.75	0.007
P50225	Sulfotransferase 1A1	SULT1A1	1.50	0.007
P46939	Utrophin	UTRN	1.15	0.007
Q9P0S3	ORM1-like protein 1	ORMDL1	0.71	0.008
Q05469	Hormone-sensitive lipase	LIPE	0.57	0.008
Q15366	Poly(rC)-binding protein 2	PCBP2	1.34	0.008
Q8N5G0	Small integral membrane protein 20	SMIM20	0.75	0.010
Q13443	Disintegrin and metalloproteinase domain-containing protein 9	ADAM9	0.65	0.010
Q12955	Ankyrin-3	ANK3	0.53	0.010
Q15006	ER membrane protein complex subunit 2	EMC2	0.81	0.010
Q9UPN3	Microtubule-actin cross-linking factor 1, isoforms 1/2/3/5	MACF1	1.26	0.010
P26006	Integrin alpha-3	ITGA3	1.33	0.011
Q02338	D-beta-hydroxybutyrate dehydrogenase, mitochondrial	BDH1	0.78	0.011
Q6IAN0	Dehydrogenase/reductase SDR family member 7B	DHRS7B	0.77	0.011
Q9BWS9	Chitinase domain-containing protein 1	CHID1	1.28	0.012
O95232	Luc7-like protein 3	LUC7L3	0.79	0.012
Q5SSJ5	Heterochromatin protein 1-binding protein 3	HP1BP3	1.28	0.013
Q92765	Secreted frizzled-related protein 3	FRZB	1.93	0.013
P23229	Integrin alpha-6	ITGA6	1.29	0.013
O75781	Paralemmin-1	PALM	1.52	0.014
P31946	14-3-3 protein beta/alpha	YWHAB	1.31	0.015
P35222	Catenin beta-1	CTNNB1	1.23	0.015
Q5EB52	Mesoderm-specific transcript homolog protein	MEST	1.99	0.016
P22695	Cytochrome b-c1 complex subunit 2, mitochondrial	UQCRC2	1.27	0.016
Q99439	Calponin-2	CNN2	1.37	0.017
O43759	Synaptogyrin-1	SYNGR1	0.71	0.017
P67936	Tropomyosin alpha-4 chain	TPM4	1.29	0.018
P09493	Tropomyosin alpha-1 chain	TPM1	1.85	0.018
P63218	Guanine nucleotide-binding protein G(I)/G(S)/G(O) subunit gamma-5	GNG5	1.45	0.019
Q8NBU5	ATPase family AAA domain-containing protein 1	ATAD1	1.33	0.019
Q6P4A7	Sideroflexin-4	SFXN4	0.75	0.019
P27797	Calreticulin	CALR	1.27	0.019
P00167	Cytochrome b5	CYB5A	1.68	0.019
P47985	Cytochrome b-c1 complex subunit Rieske, mitochondrial	UQCRFS1	1.31	0.019
Q16822	Phosphoenolpyruvate carboxykinase [GTP], mitochondrial	PCK2	0.77	0.019
Q93008	Probable ubiquitin carboxyl-terminal hydrolase FAF-X	USP9X	0.59	0.019
Q02509	Otoconin-90	OC90	1.74	0.019
O15321	Transmembrane 9 superfamily member 1	TM9SF1	1.27	0.021
P83731	60S ribosomal protein L24	RPL24	0.83	0.021
P13284	Gamma-interferon-inducible lysosomal thiol reductase	IFI30	0.68	0.022
O60427	Fatty acid desaturase 1	FADS1	1.26	0.022
Q01995	Transgelin	TAGLN	2.01	0.022
O95861	3'(2'),5'-bisphosphate nucleotidase 1	BPNT1	1.12	0.022

Q9NR28	Diablo homolog, mitochondrial	DIABLO	0.76	0.023
O14548	Cytochrome c oxidase subunit 7A-related protein, mitochondrial	COX7A2L	1.30	0.024
Q9H061	Transmembrane protein 126A	TMEM126A	0.78	0.024
Q14289	Protein-tyrosine kinase 2-beta	PTK2B	1.85	0.024
P60660	Myosin light polypeptide 6	MYL6	1.28	0.025
Q9BUN8	Derlin-1	DERL1	0.67	0.025
Q5TFQ8	Signal-regulatory protein beta-1 isoform 3	SIRPB1	1.51	0.025
O15031	Plexin-B2	PLXNB2	1.14	0.025
P19105	Myosin regulatory light chain 12A	MYL12A	1.27	0.026
P21291	Cysteine and glycine-rich protein 1	CSRP1	1.45	0.026
O96011	Peroxisomal membrane protein 11B	PEX11B	0.72	0.026
P54760	Ephrin type-B receptor 4	EPHB4	1.74	0.026
Q14165	Malectin	MLEC	1.14	0.027
P06132	Uroporphyrinogen decarboxylase	UROD	1.45	0.027
Q16270	Insulin-like growth factor-binding protein 7	IGFBP7	1.52	0.027
P99999	Cytochrome c	CYCS	0.75	0.027
Q09666	Neuroblast differentiation-associated protein AHNAK	AHNAK	1.36	0.028
O60506	Heterogeneous nuclear ribonucleoprotein Q	SYNCRIP	0.80	0.028
P61604	10 kDa heat shock protein, mitochondrial	HSPE1	0.73	0.029
P37840	Alpha-synuclein	SNCA	1.13	0.030
P07355	Annexin A2	ANXA2	1.27	0.030
P13073	Cytochrome c oxidase subunit 4 isoform 1, mitochondrial	COX4I1	1.43	0.030
P42765	3-ketoacyl-CoA thiolase, mitochondrial	ACAA2	0.73	0.031
Q16531	DNA damage-binding protein 1	DDB1	1.24	0.031
Q5SWX8	Protein odr-4 homolog	ODR4	0.83	0.031
Q13724	Mannosyl-oligosaccharide glucosidase	MOGS	1.23	0.031
Q9NP72	Ras-related protein Rab-18	RAB18	0.86	0.031
P62263	40S ribosomal protein S14	RPS14	0.89	0.031
Q8NFW8	N-acylneuraminate cytidylyltransferase	CMAS	0.89	0.032
P11216	Glycogen phosphorylase, brain form	PYGB	1.20	0.032
O00410	Importin-5	IPO5	0.74	0.032
P35637	RNA-binding protein FUS	FUS	0.55	0.032
Q96A49	Synapse-associated protein 1	SYAP1	0.75	0.033
Q9Y3D6	Mitochondrial fission 1 protein	FIS1	0.82	0.034
P23468	Receptor-type tyrosine-protein phosphatase delta	PTPRD	1.32	0.034
P52758	2-iminobutanoate/2-iminopropanoate deaminase	RIDA	0.80	0.034
P15559	NAD(P)H dehydrogenase [quinone] 1	NQO1	0.62	0.034
Q9Y696	Chloride intracellular channel protein 4	CLIC4	1.42	0.034
Q9Y5M8	Signal recognition particle receptor subunit beta	SRPRB	0.83	0.036
P19022	Cadherin-2	CDH2	1.29	0.036
P09382	Galectin-1	LGALS1	1.49	0.036
Q13308	Inactive tyrosine-protein kinase 7	PTK7	1.21	0.037
P35221	Catenin alpha-1	CTNNA1	1.16	0.037
Q15293	Reticulocalbin-1	RCN1	1.24	0.037
Q9UMS4	Pre-mRNA-processing factor 19	PRPF19	1.18	0.037
Q14699	Raftlin	RFTN1	1.46	0.037
O94875	Sorbin and SH3 domain-containing protein 2	SORBS2	1.43	0.037
P35237	Serpin B6	SERPINB6	1.34	0.038
Q9NZI8	Insulin-like growth factor 2 mRNA-binding protein 1	IGF2BP1	1.51	0.039
Q8TB22	Spermatogenesis-associated protein 20	SPATA20	0.56	0.041
Q00059	Transcription factor A, mitochondrial	TFAM	0.73	0.041
O15460	Prolyl 4-hydroxylase subunit alpha-2	P4HA2	1.22	0.041
A0FGR8	Extended synaptotagmin-2	ESYT2	1.22	0.042
P07339	Cathepsin D	CTSD	0.77	0.042
P62854	40S ribosomal protein S26	RPS26	0.71	0.042
Q86X29	Lipolysis-stimulated lipoprotein receptor	LSR	1.18	0.042
P49419	Alpha-aminoadipic semialdehyde dehydrogenase	ALDH7A1	0.87	0.042
Q9BS26	Endoplasmic reticulum resident protein 44	ERP44	1.13	0.042
Q96LJ7	Dehydrogenase/reductase SDR family member 1	DHRS1	1.19	0.043
P61586	Transforming protein RhoA	RHOA	1.10	0.044
P51659	Peroxisomal multifunctional enzyme type 2	HSD17B4	0.78	0.045
Q1KMD3	Heterogeneous nuclear ribonucleoprotein U-like protein 2	HNRNPUL2	1.25	0.045
P42126	Enoyl-CoA delta isomerase 1, mitochondrial	ECI1	0.80	0.045
P30443	HLA class I histocompatibility antigen, A-1 alpha chain	HLA-A	1.22	0.045
P25705	ATP synthase subunit alpha, mitochondrial	ATP5A1	0.89	0.045
P09669	Cytochrome c oxidase subunit 6C	COX6C	1.70	0.045
Q06787	Synaptic functional regulator FMR1	FMR1	0.77	0.047
P47755	F-actin-capping protein subunit alpha-2	CAPZA2	1.24	0.047
Q14BN4	Sarcolemmal membrane-associated protein	SLMAP	1.66	0.048
O94973	AP-2 complex subunit alpha-2	AP2A2	0.84	0.048
P53634	Dipeptidyl peptidase 1	CTSC	0.56	0.048
O76094	Signal recognition particle subunit SRP72	SRP72	0.78	0.048
P62750	60S ribosomal protein L23a	RPL23A	0.83	0.048
Q9Y285	Phenylalanine--tRNA ligase alpha subunit	FARSA	0.86	0.049
O00754	Lysosomal alpha-mannosidase	MAN2B1	0.77	0.049
O95302	Peptidyl-prolyl cis-trans isomerase FKBP9	FKBP9	1.28	0.049
Q9H223	EH domain-containing protein 4	EHD4	1.14	0.050
P07948	Tyrosine-protein kinase Lyn	LYN	1.27	0.050

Supplementary Table 3. IPA pathway analysis for diseases and biological functions for the significant proteins with p-value <0.05.
Annotations with increased (>1.5, green) or decreased (<-1.5, red) functions based on activation z-score shown.

Diseases or Functions Annotation	p-Value	Activation Z-score	# Proteins
Microtubule dynamics	4.25E-04	2.775	26
Migration of endothelial cells	5.99E-04	2.747	11
Formation of cellular protrusions	1.12E-04	2.667	23
Binding of endothelial cells	1.79E-03	2.607	7
Invasion of cells	7.99E-05	2.554	24
Organization of cytoplasm	1.71E-05	2.51	35
Organization of cytoskeleton	2.05E-04	2.51	30
Migration of cells	1.09E-03	2.502	37
Development of neurons	2.07E-03	2.444	18
Cell movement of endothelial cells	3.49E-04	2.429	12
Reorganization of cytoskeleton	2.99E-04	2.407	8
Cell spreading	2.89E-04	2.359	10
Cell viability	4.25E-03	2.342	26
Binding of fibroblast cell lines	1.67E-03	2.207	5
Neuritogenesis	1.90E-04	2.205	17
Cell movement	3.60E-04	2.203	42
Migration of vascular endothelial cells	4.92E-03	2.201	6
Interaction of endothelial cells	4.27E-04	2.158	8
Development of vasculature	4.44E-04	2.112	24
Angiogenesis	2.63E-03	2.112	20
Fibrogenesis	5.94E-03	2.098	11
Cell survival	4.63E-03	2.057	27
Vasculogenesis	5.15E-04	1.957	19
Synthesis of fatty acid	3.57E-03	1.912	9
Movement Disorders	2.85E-03	1.899	22
Axonogenesis	1.31E-03	1.875	8
Formation of actin stress fibers	1.82E-03	1.829	8
Endothelial cell development	2.83E-04	1.778	12
Development of epithelial tissue	2.63E-03	1.778	13
Attachment of cells	9.70E-04	1.732	6
Synthesis of eicosanoid	3.85E-03	1.633	7
Formation of cytoskeleton	1.59E-03	1.627	11
Motor dysfunction or movement disorder	1.57E-03	1.571	23
Proliferation of endothelial cells	4.15E-03	1.556	9
Anoikis	5.17E-04	-1.528	6
Senescence of fibroblast cell lines	6.36E-03	-1.934	5
Oxidation of lipid	3.09E-03	-1.983	7

Supplementary Table 4. Upstream regulators of the disease associated pathways.
Regulators with increased, positive (z-score >1.5 green) correlation for the protein expression and decreased, negative correlation (z-score <-1.5, red) shown.

Upstream Regulator	Molecule Type	Activation Z-score	p-value of overlap
TGFB1	growth factor	3.241	2.98E-06
calcitriol	chemical drug	2.813	2.09E-02
AGT	growth factor	2.359	5.41E-03
TNF	cytokine	2.245	3.67E-04
hexachlorobenzene	chemical toxicant	2.236	5.50E-05
lomustine	chemical drug	2.236	9.62E-05
triamterene	chemical drug	2.236	1.11E-04
allopurinol	chemical drug	2.236	3.47E-04
fenamic acid	chemical reagent	2.219	1.38E-04
vancomycin	biologic drug	2.219	4.09E-04
E2F1	transcription regulator	2.195	6.50E-02
SPP1	cytokine	2	1.98E-03
ERG	transcription regulator	2	3.09E-03
tanespimycin	chemical drug	2	9.78E-03
F2R	G-protein coupled receptor	1.982	6.49E-03
SMAD3	transcription regulator	1.981	2.69E-02
phenylbutazone	chemical drug	1.98	9.07E-04
thioacetamide	chemical toxicant	1.98	2.07E-03
IL1B	cytokine	1.969	4.57E-01
IL6	cytokine	1.969	2.75E-01
E. coli B4 lipopolysaccharide	chemical toxicant	1.964	1.48E-01
INS	other	1.961	5.10E-03
POU5F1	transcription regulator	1.949	2.20E-01
lenalidomide	chemical drug	1.925	4.51E-02
CEBPB	transcription regulator	1.89	3.26E-03
LONP1	peptidase	1.886	7.85E-06
cisplatin	chemical drug	1.841	1.78E-02
Ins1	other	1.667	1.67E-05
SYVN1	transporter	1.633	4.50E-04
TCF7L2	transcription regulator	1.633	3.27E-02
NFKBIA	transcription regulator	1.626	4.62E-03
lipopolysaccharide	chemical drug	1.565	6.27E-03
IFNG	cytokine	1.54	3.69E-03
L-glutamic acid	chemical - endogenous mammalian	1.446	8.83E-04
PP2/AG1879 tyrosine kinase inhibitor	chemical - kinase inhibitor	-1.732	2.40E-03
PPARD	ligand-dependent nuclear receptor	-1.862	7.02E-02
rosiglitazone	chemical drug	-1.862	3.69E-03
HNF4A	transcription regulator	-1.937	3.43E-05
ARNT	transcription regulator	-1.964	1.88E-03
TSC2	other	-2	1.19E-02
cyclic AMP	chemical - endogenous mammalian	-2	4.01E-02
PPARG	ligand-dependent nuclear receptor	-2.022	2.27E-03
HOXD10	transcription regulator	-2.236	8.92E-05
SP600125	chemical - kinase inhibitor	-2.646	9.11E-04
MYCN	transcription regulator	-3.065	1.37E-07